Helsinki University of Technology Laboratory of Computational Engineering Publications
Teknillisen korkeakoulun Laskennallisen tekniikan laboratorion julkaisuja
Espoo 2007 Report B64

COMPUTATIONAL METHODS FOR BAYESIAN ESTIMATION OF NEUROMAGNETIC SOURCES

Toni Auranen

TEKNILLINEN KORKEAKOULU
TEKNISKA HÖGSKOLAN
HELSINKI UNIVERSITY OF TECHNOLOGY
TECHNISCHE UNIVERSITÄT HELSINKI
UNIVERSITÉ DE TECHNOLOGIE D'HELSINKI

Helsinki University of Technology Laboratory of Computational Engineering Publications
Teknillisen korkeakoulun Laskennallisen tekniikan laboratorion julkaisuja
Espoo 2007 Report B64

COMPUTATIONAL METHODS FOR BAYESIAN ESTIMATION OF NEUROMAGNETIC SOURCES

Toni Auranen

Dissertation for the degree of Doctor of Science in Technology to be presented with due permission of the Department of Electrical and Communications Engineering, Helsinki University of Technology, for public examination and debate in Auditorium S4 at Helsinki University of Technology (Espoo, Finland) on the 27th of October, 2007, at 12 noon.

Helsinki University of Technology
Department of Electrical and Communications Engineering
Laboratory of Computational Engineering

Teknillinen korkeakoulu
Sähkö- ja tietoliikennetekniikan osasto
Laskennallisen tekniikan laboratorio

Distribution:
Helsinki University of Technology
Laboratory of Computational Engineering
http://www.lce.hut.fi
P.O. Box 9203
FI-02015 TKK
FINLAND
Tel. +358-9-451 4826
Fax. +358-9-451 4830
http://www.lce.hut.fi

Online in PDF format: http://lib.hut.fi/Diss/2007/isbn9789512289547/

E-mail: Toni.Auranen@tkk.fi

ISBN 978-951-22-8953-0 (printed)
ISBN 978-951-22-8954-7 (PDF)
ISSN 1455-0474
PicaSet Oy
Helsinki 2007

Abstract

The electromagnetic inverse problem in human brain research consists of determining underlying source currents in the brain based on measurements outside the head. Solution to the inverse problem is ambiguous, necessitating the use of prior information and modeling assumptions for obtaining reasonable inverse estimates. In this study, we create new and improve existing computational methods for estimating neuromagnetic sources in the human brain.

One straightforward way of incorporating presumptions to this problem is to formulate it in a probabilistic Bayesian manner. Bayesian statistics is largely based on modeling uncertainties associated with parameters constituting the model by representing them with probability distributions. In this work, existing neuroscientific knowledge and information from anatomical and functional magnetic resonance imaging are used as prior assumptions in model implementation.

The neuromagnetic inverse problem is resolved with two different approaches. First, we perform the analysis using distributed source current modeling and infer some arbitrary parameter choices and the source currents from the measurement data by using numerical sampling methods. We apply similar strategies to cortically constrained current dipole localization and suggest using functional magnetic resonance imaging data for guiding the sampling algorithm. The models are tested with simulated and measured data.

The presented methods are rather automatic, yielding plausible and robust inverse estimates of cortical current sources. With the spatiotemporal dipole localization model, the inclusion of functional magnetic resonance imaging data improves performance of the numerical sampling method. However, apparent multimodality of the parameter posterior distribution causes complications especially with empirical data.

We suggest using loose cortical orientation constraints for smoothing down the complicated posterior distribution instead of marginal improvements to the sampling scheme. This might help to overcome the somewhat limited mixing properties of the sampling algorithm and ease the inconvenient multimodality of the posterior distribution.

Tiivistelmä

Ihmisaivojen tutkimukseen liittyvällä sähkömagneettisella käänteisongelmalla tarkoitetaan aivojen virtalähteiden paikantamista pään ulkopuolisten mittausten perusteella. Ongelmaan ei ole yksikäsitteistä ratkaisua, joten mallintamisessa on käytettävä ennakko-oletuksia järkevien ratkaisujen tuottamiseksi. Tässä tutkimuksessa kehitämme uusia ja parannamme olemassaolevia laskennallisia menetelmiä aivoissa syntyvien magneettikenttiä tuottavien lähteiden paikantamiseksi.

Kenties yksinkertaisin tapa lisätä ennakko-oletuksia tähän ongelmaan on käyttää bayesilaista mallintamista. Bayesilainen tilastotiede perustuu pitkälti parametrien epävarmuuksien mallintamiseen ja esittämiseen todennäköisyysjakaumin. Työn mallien muodostamisessa käytetään apuna aivojen toiminnallisesta ja rakenteellisesta magneettikuvauksesta saatavaa neurotieteellistä ennakkotietoa.

Sähkömagneettisen käänteisongelman ratkaisuun käytämme kahta eri menetelmää. Aluksi analysoimme aivojen pinnalle muodostettuja virtalähdejakaumamalleja ja pyrimme laskennallisia otantamenetelmiä käyttäen arvioimaan virtojen sekä muuten etukäteen mielivaltaisesti valittavien parametrien arvoja mittausaineistosta. Sovellamme samantyyppistä otantamenetelmää malliin, missä dipolaarisia virtalähteitä rajoittaa aivojen kuorikerroksen anatomia ja fysiologia. Ehdotamme lisäksi toiminnallisen magneettikuvauksen tuottaman mittausaineiston käyttöä otantamenetelmän apuna. Malleja testataan sekä simuloidulla että kokeellisella mittausaineistolla.

Kehitetyt menetelmät ovat hyvin automaattisia ja tuottavat järkeviä ratkaisuja magneettisten mittausten lähteiksi. Dipolaaristen virtalähteiden paikallis-ajalliseen määrittämiseen käytetyn otantamenetelmän suorituskyky parantuu toiminnallisesta magneettikuvauksesta saatavan tiedon avulla. Mallin parametrien todennäköisyysjakauma on kuitenkin selvästi monihuippuinen aiheuttaen ongelmia erityisesti kokeellisen mittausaineiston kanssa.

Otantamenetelmän parannusten sijaan ehdotamme väljempien aivojen kuorikerroksen anatomiaan perustuvien rajoitteiden käyttöä, jolloin itse parametrien todennäköisyysjakauma saattaa muuttua helpommin käsiteltäväksi. Tämä parantanee myös nykyisen otantamenetelmän tehokkuutta tässä ongelmassa ja helpottaa siten monihuippuisten jakaumien jatkokäsittelyä.

List of abbreviations

A1	Primary auditory cortex
BEM	Boundary-element model
BOLD	Blood oxygenation level dependent
ECD	Equivalent current dipole
EEG	Electroencephalography/Electroencephalogram
EF	Evoked field
fMRI	Functional magnetic resonance imaging
LH	Left hemisphere
M1	Primary motor cortex
MAP	Maximum *a posteriori*
MCE	Minimum-current estimate
MCMC	Markov chain Monte Carlo
MEG	Magnetoencephalography/Magnetoencephalogram
MNE	Minimum-norm estimate
MR	Magnetic resonance
MRI	Magnetic resonance imaging
PET	Positron emission tomography
RF	Radio frequency
RH	Right hemisphere
RJMCMC	Reversible jump Markov chain Monte Carlo
S1	Primary somatosensory areas
SNR	Signal-to-noise ratio
SVD	Singular value decomposition
V1	Primary visual cortex
V2	First visual association area
V3/VP	Visual area located immediately in front of V2
V5/MT	Middle temporal visual area
VB	Variational Bayesian

Preface

This thesis was prepared in the Laboratory of Computational Engineering at the Helsinki University of Technology during 2003–2007. My research was funded by the Academy of Finland under the Centre of Excellence projects in Computational Science and Engineering (2000–2005) and in Computational Complex Systems Research (2006–2011), and by the National Technology Agency (TEKES). My studies were also financially supported by Jenny and Antti Wihuri Foundation and Foundation for Promoting Technology (Tekniikan edistämissäätiö).

First, I would like to thank Prof. Mikko Sams for his supervision and support during my research. Professors Kimmo Kaski, Jouko Lampinen, and Jukka Tulkki deserve a big portion of my appreciation for creating an enjoyable multidisciplinary research environment. I cordially acknowledge our laboratory's affiliations to the Advanced Magnetic Imaging Centre and the Brain Research Unit of the Low Temperature Laboratory, both at the HUT, and thank their respective personnel led by Prof. Riitta Hari. My sincere thanks go to Prof. Risto Ilmoniemi and Dr. Seppo Ahlfors for reviewing this thesis and providing insightful comments.

I am grateful to Dr. Iiro Jääskeläinen and Dr. Aki Vehtari for their wisdom on neuroscience and Bayesian modeling, respectively. I feel most indebted to M.Sc. Aapo Nummenmaa as my closest brother-in-arms, without whom this would not have been possible. Aapo along with Prof. Matti Hämäläinen, Dr. Simo Vanni, and the rest of my co-authors are praised for their contribution. With various issues, I thank Dr. Johanna Pekkola, Dr. Ville Ojanen, M.D. Marja Balk, M.Soc.Sc. Eeva Lampinen, M.Sc. Arto Selonen, and many other past and present personnel of our laboratory. You all kept the wheels turning!

Finally, I want to thank my closest friends and family members, and most of all, my wife Minna for the altruistic support she has given me throughout this time. I dedicate this thesis to Raimo, Kirsti, Minna, Anni, Juho, and Tero.

Espoo, September 5, 2007

Toni Auranen

List of publications and author's research contributions

This dissertation consists of an overview and the following publications:

I Auranen, T., Nummenmaa, A., Hämäläinen, M. S., Jääskeläinen, I. P., Lampinen, J., Vehtari, A., and Sams, M. (2005). Bayesian analysis of the neuromagnetic inverse problem with ℓ^p-norm priors. *NeuroImage*, 26(3):870–884.

II Nummenmaa, A., Auranen, T., Hämäläinen, M. S., Jääskeläinen, I. P., Lampinen, J., Sams, M., and Vehtari, A. (2007). Hierarchical Bayesian estimates of distributed MEG sources: Theoretical aspects and comparison of variational and MCMC methods. *NeuroImage*, 35(2):669–685.

III Nummenmaa, A., Auranen, T., Hämäläinen, M. S., Jääskeläinen, I. P., Sams, M., Vehtari, A., and Lampinen, J. (2007). Automatic relevance determination based hierarchical Bayesian MEG inversion in practice. *NeuroImage*, 37(3):876–889.

IV Auranen, T., Nummenmaa, A., Hämäläinen, M. S., Jääskeläinen, I. P., Lampinen, J., Vehtari, A., and Sams, M. (2007). Bayesian inverse analysis of neuromagnetic data using cortically constrained multiple dipoles. *Human Brain Mapping*, 28(10):979–994.

V Auranen, T., Nummenmaa, A., Vanni, S., Vehtari, A., Hämäläinen, M. S., Lampinen, J., and Jääskeläinen, I. P. (2007). Automatic fMRI-guided MEG multidipole localization for visual responses. *Helsinki University of Technology Laboratory of Computational Engineering Publications*, Report B63, ISBN 978-951-22-8952-3.

The first author had principal responsibility for preparing and writing of the manuscripts, while others contributed with suggestions and modifications of the text. Co-authors contributed especially in conceptions and initiation of this research.

I was the principal author in Publications I, IV, and V. In Publication I, the first and second author jointly performed background research and model specification. In Publication I, data simulations, experimental setup/empirical data acquisition, model implementation, and data analyses were mostly carried out by myself with assistance from the second author. In Publications IV and V, experimental setup/empirical data acquisition and model specification were done by myself and assisted in some parts by the second author. In these works, I solely prepared data simulations, implemented the models, and performed all data analyses. The third author of Publication V contributed equally with the second author to the experimental setup/empirical data acquisition and writing process of this particular work.

In Publications II and III, I had the principal responsibility in data simulations and experimental setup/empirical data acquisition while the first author had the principal responsibility in other parts. In these works, I also assisted in the preparation of manuscripts and background considerations.

In addition, I have developed a core set of MATLAB functions used to import, preprocess, analyze, and visualize the data investigated in all the included publications.

Contents

Chapter 1

Introduction

Prior to the 20th century, functional research of human brain was mainly conducted by relating behavioral deficits with extent and loci of brain lesions. Such explorations form still the basis of our present knowledge of functional anatomy of the human brain. Since those times, noninvasive brain measurement techniques have taken huge steps. Today, researchers have the opportunity to choose from temporally accurate electromagnetic recordings of neural activity with electroencephalography (EEG) and *magnetoencephalography* (MEG), to spatially focal mappings based on nuclear magnetic resonance, for example.

Magnetic resonance imaging (MRI) is currently one of the best techniques for studying the anatomy of the living brain. This method has gained a huge momentum in the past two or three decades and its developers were awarded the 2003 Nobel Prize in Medicine. Due to its usefulness also as a clinical tool, MRI has already earned its place in many hospitals and research facilities. For the functional studies of the brain, MEG has gained popularity along with *functional magnetic resonance imaging* (fMRI). However, both MEG and EEG require thorough analyses for solving the so-called *electromagnetic inverse problem* to localize *neuronal sources* in the brain. For some years, one of the hot topics in this field has been the efficient combination of different imaging modalities (*e.g.*, MEG and fMRI) for producing both temporally and spatially exquisite solutions.

The above-mentioned state-of-the-art methods are used in neuroscience, for example, in investigating brain mechanisms of human sensory processing. The visual, somatosensory, and auditory processing networks have been an area of considerable interest, because these sensory modalities are of special importance to humans. With the modern imaging technologies and by using sophisticated experimental designs, however, it is also possible to study more cognitive issues such as attention and memory.

In this work, the electromagnetic inverse problem of brain signal analysis is studied using *Bayesian statistics* and *computational methods*. The computa-

tional methods are mainly based on Markov chain Monte Carlo (MCMC) sampling. MCMC sampling is often used in Bayesian inference with complicated models when the associated integration of high-dimensional probability distributions turns out to be infeasible or when suitable analytical approximations cannot be constructed. Both anatomical and functional MRI data are used as prior information in the inverse modeling schemes. In the pursuit to develop novel methods for neuroscience research, validation of the models is done using empirical and simulated MEG and fMRI data.

This thesis consists of an overview and five peer-reviewed publications organized by subject matter. The inverse problem is first studied in Publications I, II, and III from the point of view of *distributed source current estimates* using MCMC sampling and variational Bayesian (VB) method. In the distributed methods the brain is discretized to a predefined number of source space points. The number of these points can be several thousand, and current estimates are calculated to all of them. In Publications IV and V, the activity underlying the magnetic field changes is modeled with a small varying number of *equivalent current dipoles* (ECD). Publication IV deals with the utilization of MRI anatomical information with dipole fitting. In Publication V, a new way of incorporating fMRI data to the MEG inverse analysis is proposed. Potential complications of applying intensive computational methods to such a complex problem as the MEG inverse problem are addressed in all the publications.

Chapter 2 introduces the necessary concepts and reviews the relevant literature. The aims of the study are described in Chapter 3. Chapter 4 is an introduction to the specific experimental procedures and data simulations along with a short description of the analysis environment used in the thesis. The models and results from the experiments are presented in Chapter 5. Before summary, the main findings and future goals of this research are discussed.

Chapter 2

Review of literature

2.1 Bayesian data analysis

The models used to solve the electromagnetic inverse problem in this thesis are treated with *Bayesian inference* (see also, Section 2.3.4 on page 16). It is a probabilistic formalism in which observables y and parameters of the model θ are all treated as random variables. A *joint probability* model for the parameters and the observables is constructed and always conditioned to some modeling assumptions $\mathcal{M}$ made by the analyst. The key feature of Bayesian data analysis is that statistical conclusions about the parameters of interest θ or predicted observables $\tilde{y}$ are made in probability statements (see, *e.g.*, Gelman et al., 2003; Bernardo and Smith, 2000, for more details).

The joint probability model, $p(\theta, y|\mathcal{M})$, can be written as a product of a *likelihood* function for the data given the parameters, $p(y|\theta, \mathcal{M})$, and a *prior distribution* for the parameters, $p_0(\theta|\mathcal{M})$.

$$p(\theta, y|\mathcal{M}) = p(y|\theta, \mathcal{M}) \cdot p_0(\theta|\mathcal{M}) \tag{2.1}$$

Conditioning to y, the posterior distribution for θ is given by the Bayes' rule (*e.g.*, Gelman et al., 2003)

$$p(\theta|y, \mathcal{M}) = \frac{p(y|\theta, \mathcal{M}) \cdot p_0(\theta|\mathcal{M})}{p(y|\mathcal{M})}, \tag{2.2}$$

where $p(y|\mathcal{M}) = \int p(y|\theta, \mathcal{M}) \cdot p_0(\theta|\mathcal{M}) \mathrm{d}\theta$ is a normalization factor describing the probability of data y under model $\mathcal{M}$ for all possible parameter values. With a fixed set of measurement data y, this factor can be omitted, yielding unnormalized posterior density

$$p(\theta|y, \mathcal{M}) \propto p(y|\theta, \mathcal{M}) \cdot p_0(\theta|\mathcal{M}). \tag{2.3}$$

The marginal distribution (or evidence) of data is often called prior predictive distribution $p(y|\mathcal{M}) =^1 p(y) = \int p(y|\theta) \cdot p_0(\theta) \mathrm{d}\theta$. After the data have been observed, we can make predictions of the unknown (future) observables $\tilde{y}$ from the same model. Following the same logic as before, we arrive at the *posterior predictive distribution* of $p(\tilde{y}|y) = \int p(\tilde{y}|\theta) \cdot p(\theta|y) \mathrm{d}\theta$. Posterior predictive analysis can be used, for instance, in choosing the optimal model (*e.g.*, Gelfand and Ghosh, 1998). Model selection was performed in Publication I.

One significant virtue of the Bayesian framework is that new parameters and prior information can relatively easily be incorporated into the model. This is useful in constructing models for the electromagnetic inverse problem, and also leads to the possibility of adding intuitive hierarchy, meaning that additional prior distributions can be assigned to the parameters of prior distributions and even further (see, Publications II and III). Doing so, the researcher is able to model uncertainty to ambiguous parameters or rigorous information to those that are unambiguous. Such hierarchical models with several higher-level parameters (*i.e.*, *hyperparameters*) have been widely used in statistical inference problems.

In order to make probabilistic inferences on the parameters, such as the amplitude and location of the electric currents in the brain when considering the electromagnetic inverse problem (see, Section 2.3), it is necessary to compute some characteristic quantities or suitable marginal densities based on their poste-

[1] In the rest of this section, notation $\mathcal{M}$ is omitted for clarity, although it is important to bear in mind that a model is always formulated *given* some modeling assumptions.

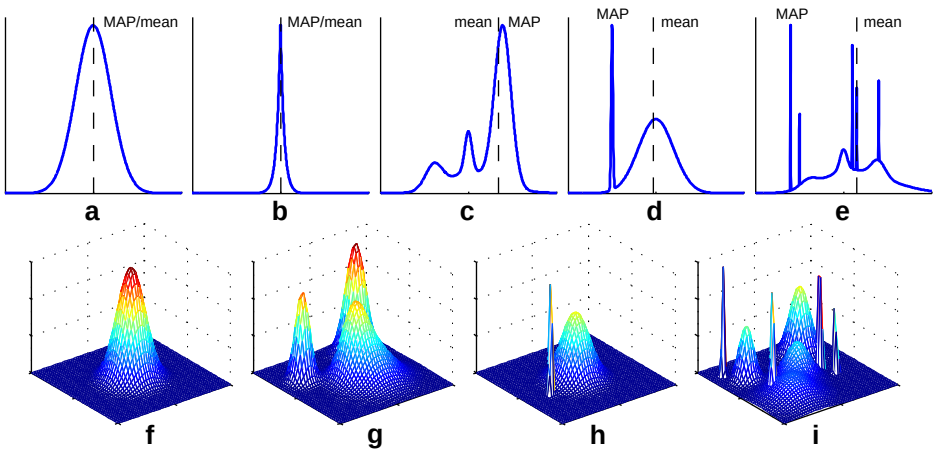

Figure 2.1: Differently shaped one- and two-dimensional distributions. Distributions **a**, **b**, and **f** have only one global maximum while the rest have several local maxima. Distributions **e** and **i** have several sharp spikes in addition to the varying landscape.

rior distribution. For example, a distribution is often described by the parameters maximizing it, that is, the *maximum a posteriori* (MAP) estimate, or by its mean expectation value (Fig. 2.1). Often, the posterior distribution turns out to be *multimodal* (*i.e.*, there are several local maxima) or the posterior may be very spiky and in the worst case both (Fig. 2.1e). In the unimodal case (Figs. 2.1a, 2.1b, and 2.1f) the MAP estimate often coincides with the most probability mass, but with multimodal distributions the "best solution" is not nesessarily the MAP estimate as most probability mass may be located elsewhere (Figs. 2.1d and 2.1h).

In this thesis, the posterior distribution is a function of several variables with much more difficult shape than the one- and two-dimensional examples in Fig. 2.1. For example, in Publication I, the number of parameters in the model is equivalent to the number of points in the discretized brain (several hundred). Because of the high dimensionality of the associated problem or intractability of the integrals involved in the marginalization or computation of expectation values, numerical methods are typically needed. Most computational methods used in this work relate to the numerical sampling of the posterior distribution (Eq. 2.3) with Markov chain Monte Carlo methods. In the analyses, we are able to calculate the inverse estimates for the source current location and amplitude from the numerical samples of the parameters. Notably, the posterior distribution of the parameters is heavily multimodal especially with the dipole models in Publications IV and V.

2.1.1 Markov chain Monte Carlo methods

MCMC methods (*e.g.*, Robert and Casella, 2004; Gilks et al., 1996) are based on constructing a Markov chain of numerical samples representing the target distribution, so that each sample depends only on the previous value in the chain. In Bayesian data analysis, the posterior distribution in question is set as this stationary target distribution towards which the chain *converges* (see, Fig. 2.2). The

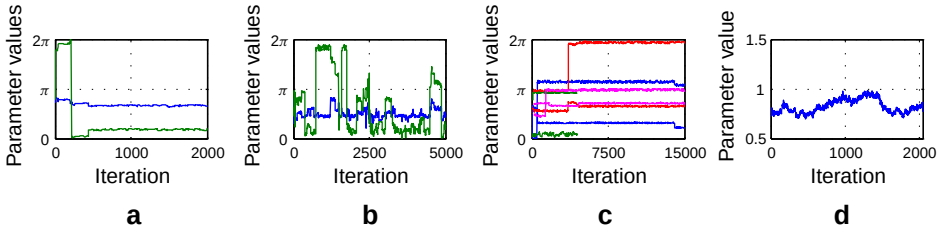

Figure 2.2: Examples of MCMC simulations. The chain of two parameters is argued to have reached convergence in about 500 iterations (**a**), whereas the distribution is clearly multimodal if the parameters switch between distinct values (**b**). Sampling becomes problematic when the parameters switch modes after a long time of stationary sampling (**c**), or when heavy autocorrelation is present (**d**).

samples obtained from simulation are representatives of the desired distribution.

There are two types of difficulties with MCMC simulations. The chain has to proceed long enough for the resulting samples to be representative of the target distribution. This is not often feasible in practice. The early iterations are also influenced by the starting point rather than the target distribution. Especially with complex and multivariate distributions, it is very difficult to determine how many samples are required for reaching convergence (*e.g.*, Brooks and Gelman, 1998). The other problem deals with correlation of the samples within the converging chain. A low number of uncorrelated (*i.e.*, independent) samples may not be enough for computing accurate characteristic quantities.

No general validation method exists for determining whether a Markov chain has converged or not. However, it can be assumed to have done so when two or more chains originating from different starting points can no longer be statistically differentiated from each other. One way of monitoring convergence is to compare variances between different segments of chains and calculate by which factor the scale of the present distribution might be reduced if the sampling was continued to infinity. This is called the potential scale reduction factor (see, *e.g.*, Gelman et al., 2003, Ch. 11.6). Often, in addition to this and time series analysis, visual verification is used to determine convergence.

Multimodal probability distributions may be very difficult to sample with MCMC methods. If the chain does not mix between all the different modes of the distribution, further inferences on the relations between the modes turns impossible. Some sampling methods, however, are designed to perform better with multimodal distributions. The standard and more advanced sampling methods used in this thesis are described in the following. Excluding *slice sampling*, these methods have been previously used in Bayesian analysis of the electromagnetic inverse problem (see, Section 2.3.4, for references).

Metropolis–Hastings

The Metropolis–Hastings algorithm (Metropolis et al., 1953; Hastings, 1970) is a numerical sampling method based on the rejection or acceptance of proposed parameter values according to an *acceptance ratio*. In this thesis, Metropolis–Hastings is used for sampling dipole locations in Publications IV and V. The algorithm produces random walk converging towards a specified (unnormalized) target distribution, such as the posterior probability distribution of Eq. 2.3. Let us assume a random initial parameter sample θ_{t-1} and a probability density of $p(\theta|y)$. At step t, a new sample θ^* is proposed according to some jumping rule, $p_J(\theta^*|\theta_{t-1})$. This sample is set as the next sample in the Markov chain, $\theta_t = \theta^*$, with probability

$$\min\left\{1,\ \frac{p(\theta^*|y)\,p_J(\theta_{t-1}|\theta^*)}{p(\theta_{t-1}|y)\,p_J(\theta^*|\theta_{t-1})}\right\}. \tag{2.4}$$

Otherwise, the jump is rejected and the old value is repeated in the chain, $\theta_t = \theta_{t-1}$. The proposal distribution $p_J(\cdot)$ does not need to be symmetric as long as detailed balance holds and the jump is reversible. This has to be accounted for in the calculation of the acceptance ratio. The obtained sequence of samples can now be used to approximate the target distribution with a histogram, for instance, or to calculate an expectation value that would otherwise require high-dimensional (intractable) integration. A badly selected proposal distribution leads to inefficient sampling, especially with multimodal distributions.

Gibbs sampling

Gibbs sampling (Geman and Geman, 1984), used in Publication II (see, Section 5.2), is a special case of single-component Metropolis–Hastings sampling. In single-component Metropolis–Hastings, the parameter vector θ is divided into n blocks $\{\theta_1, \theta_2, \ldots, \theta_n\}$ and the blocks are sequentially updated using proposal distribution $p_{Ji}(\theta_i^*|\theta_i, \theta_{\setminus i})$. Here, θ_i is the state of the ith block and $\theta_{\setminus i}$ is the state of the blocks $1, 2, \ldots, i-1$ already updated with Metropolis–Hastings. In Gibbs sampling the proposal of a component is the full conditional distribution of the ith component given all the other components, $p_{Ji}(\theta_i^*|\theta_{\setminus i})$, yielding the proposals always accepted. The downside with Gibbs sampling is that one must be able to draw samples from the conditional distribution of each block or variable. This can be much harder than defining the joint posterior distribution.

Slice sampling

In this work, slice sampling (Neal, 2003) was used for the first time in solving the electromagnetic inverse problem using a continuous parametrization for the discrete source current locations. Slice sampling relies on the principle that one can sample uniformly under the curve of some known probability density function. It is able to adapt to local properties of the target distribution, yet requiring little tuning. Unlike in Gibbs sampling, the conditional distributions do not need to be explicitly known, and with multimodal distributions slice sampling is often more efficient than simple Metropolis–Hastings algorithm in making jumps between modes. With distributions of many parameters, each variable can be updated consecutively.

In slice sampling, a Markov chain converging to the target distribution is obtained by sampling uniformly by turns in vertical direction under the distribution density and horizontally from a slice defined by this vertical position. Let the variable to be updated be θ and $f(\theta)$ is a function proportional to the probability density of θ. In producing a chain for θ, at step t the current value θ_{t-1} is replaced with a new value θ^*. Specifically, a real value of R from $0 < R < f(\theta_{t-1})$ is drawn, defining a horizontal slice $S = \{\theta\colon\ R < f(\theta)\}$. After this, an interval

I around θ_{t-1} is selected containing much or all of the slice S. Finally, θ^* is drawn uniformly from the part of the slice within interval I and the procedure is repeated. In considering the log-posterior energy function often done for computational purposes with MCMC sampling, that is $g(\theta) = -\log(f(\theta))$, a variable $Z = \log(R) = -g(\theta_{t-1}) - E$ can be calculated to define the slice $S = \{\theta: Z < -g(\theta)\}$. Variable E is exponentially distributed with the mean of one. There are several different schemes for finding the interval I that are well covered by Neal (2003). In fact, the interval can be chosen in any way as long as the resulting Markov chain remains reversible.

Reversible jump MCMC

Reversible jump Markov chain Monte Carlo (RJMCMC) is a method for constructing a Markov chain for a probability distribution of switching dimensionality (Green, 1995). Such situations occur when the number of explanatory variables is let to alternate (*e.g.*, number of current sources in the brain is unknown). The target distribution consists, thus, of a varying number of parameters and normal MCMC schemes cannot be used.

If the current state of the Markov chain is (θ_N, N), where N is the number of parameters and also the dimensionality of parameter vector θ, the reversible jump to a new state of differing dimensionality (θ_{N^*}, N^*) is proposed with a directed jumping probability between models $p_{N\to N^*}$. The jump is accepted with probability $\min\{1, \alpha\}$, where

$$\alpha = \frac{p(y|\theta_{N^*}, N^*)\, p_0(\theta_{N^*}|N^*)\, p_{\mathcal{M}}(\theta_{N^*}, N^*)\, p_{N^*\to N}\, p_J(u^*|\theta_{N^*}, N^*, N)}{p(y|\theta_N, N)\, p_0(\theta_N|N)\, p_{\mathcal{M}}(\theta_N, N)\, p_{N\to N^*}\, p_J(u|\theta_N, N, N^*)} \times \left|\frac{\partial h_{N\to N^*}(\theta_N, u)}{\partial(\theta_N, u)}\right|. \quad (2.5)$$

$p(\cdot)$ is the sampling distribution of the model, $p_0(\cdot)$ is the prior distribution for the parameters, $p_{\mathcal{M}}(\cdot)$ is the prior probability of the model in question, and $p_J(\cdot)$ is a proposal density for a random variable u. The key feature of RJMCMC is the introduction of additional random variables u and u^* that enable the matching of parameter space dimensions of the different models. $h_{N\to N^*}$ is an invertible function defining the mapping between parameter spaces: $(\theta_{N^*}, u^*) = h_{N\to N^*}(\theta_N, u)$.

The transdimensional jumps can be constructed in any way as long as dimension matching is ensured by making both directions of a jump equally probable. Simple proposed moves can be, for example, birth (or death) of a new parameter, or a simultaneous birth (or death) of one parameter and updates of other parameter values. Due to its flexibility, reversible jump MCMC methods are applicable to model determination problems (*e.g.*, Green, 1995), for instance. With complex problems, however, finding of a suitable proposal distribution becomes extremely important for efficient sampling (*e.g.*, Brooks et al., 2003).

2.1.2 Variational Bayesian methods

Variational Bayesian methods can be used as an alternative to computationally heavy and time-consuming numerical sampling methods (for a short review on variational methods, see, *e.g.*, Ghahramani and Beal, 2001). In Publications II and III, a variational Bayesian method was compared to MCMC sampling and their properties were investigated considering the electromagnetic inverse problem, respectively. The basic idea of a VB method is to try to approximate the parameter posterior distribution $p(\theta|y)$ with a simpler trial distribution $q(\theta)$.

In the VB method, the procedure of evaluating the joint probability $p(\theta, y)$ is reformulated as a maximization problem of the *free energy*, which is defined as

$$\mathcal{F}\big(q(\theta)\big) = \int \mathrm{d}\theta q(\theta) \log\left(\frac{p(\theta, y)}{q(\theta)}\right) = \log\big(p(y)\big) - \mathrm{KL}\big(q(\theta) \| p(\theta|y)\big) \quad (2.6)$$

for the trial distribution $q(\theta)$ (*e.g.*, Sato et al., 2004). The last term in Eq. 2.6 is called the (asymmetric) Kullback-Leibler divergence

$$\mathrm{KL}\big(q(\theta) \| p(\theta|y)\big) = \int \mathrm{d}\theta q(\theta) \log\left(\frac{q(\theta)}{p(\theta|y)}\right) \quad (2.7)$$

between true and variational posteriors, $p(\theta|y)$ and $q(\theta)$, respectively. The Kullback-Leibler divergence is one possibility for measuring dissimilarity between these two distributions. Maximization of the free energy leads effectively to minimization of the Kullback-Leibler divergence, rendering $q(\theta)$ to be the closest possible analytical approximation of the true posterior $p(\theta|y)$. The optimization of the free energy can be solved, for example, using a factorization approximation in which the free energy is maximized alternately with respect to factorized parts of $q(\theta)$ (see, *e.g.*, Sato et al., 2004, for an exemplar and references).

2.2 Noninvasive brain imaging methods

Human brain imaging methods can be divided into two categories based on their level of penetration to the body. The first class of methods are essentially *invasive*, in which a contrast medium is injected to the subject. In positron emission tomography (PET) and single photon emission computed tomography, a radioactive contrast medium is used while regular computed axial tomography is based on imaging with X-rays. These methods provide three-dimensional images of the human brain.

One of the most common *noninvasive* techniques, magnetic resonance imaging, is widely used in clinical and research facilities around the world. MRI and functional MRI produce anatomical and functional information of the brain, respectively. Although MRI and fMRI can be considered to be invasive to some

extent because of the presence of strong magnetic fields and radio frequency (RF) pulses, the amount of energy absorbed by tissues is minimal and single subjects can be studied several times, unlike for example in PET.

EEG and MEG are used to noninvasively measure electric potentials and magnetic fields produced by the underlying source currents in the brain, respectively. Although EEG and MEG do not *per se* produce an image, the localized activations are often overlaid on anatomical brain images. Highly invasive subdural EEG can also be measured in humans during brain surgery.

In this thesis, data were gathered using magnetic resonance imaging, functional magnetic resonance imaging, and magnetoencephalography.

2.2.1 Magnetic resonance imaging

With magnetic resonance imaging, the spatial structure of the living brain can be determined noninvasively. This is not only important in clinical use, but also essential for basic research. For instance, the resulting volumetric images are needed in producing accurate computer models of different anatomical volumes (*e.g.*, skin, inner and outer skull) and cortical layers (*e.g.*, pial surface and white-gray matter boundary). These are required for further analyses and visualization. For the inverse analysis of MEG signals the inner skull and cortical white-gray matter boundary are of special importance as they are used in constructing the forward model (see, Section 2.3).

MRI is based on *nuclear magnetic resonance* (see, *e.g.*, Huettel et al., 2004, for details on the following). The hydrogen nucleus (*i.e.*, a single proton) has a quantum mechanical property called spin, considered to behave like a small magnet in an external field. Within this magnetic field, the protons will precess around an axis aligned either parallel (low energy) or in opposite direction (high energy) to the field. In MRI, the protons are excited with a radio frequency pulse and some of the low energy nuclei will absorb the energy and switch to high energy state. Following the pulse, the net magnetization will decay back to its equilibrium releasing the absorbed energy. The emitted energy can in turn be measured with RF coils. The signal itself is spatially encoded by varying magnetic fields with gradient coils. Different components in the frequency domain signal space can be separated and the origin of the emission determined. This is done for each of the slices of the target (*e.g.*, human head), and by inverse Fourier transform a volumetric image of the target can be produced.

The decay of the net magnetization occurs according to relaxation times T_1, T_2, and T_2^*. T_1 is called the spin-lattice or longitudinal relaxation time and it describes how long it takes for the z-component of the net magnetization to be relaxed. The spin-spin or transversal relaxation time T_2 is caused by interactions between nuclear spins. Relaxation time T_2^* includes the effect of field inhomogeneities to the spin-spin relaxation time. The separation of different tis-

sues or materials with MRI is possible because the relaxation times vary across them. When duration and detection of the applied RF pulse is varied, differently weighted images can be obtained for different purposes.

2.2.2 Functional magnetic resonance imaging

Functional MRI (*e.g.*, Ogawa et al., 1992; Bandettini et al., 1992; Belliveau et al., 1991; Kwong et al., 1992) is based on the assumption that the electrical activity in the brain is connected to *hemodynamic* changes in brain tissue (*e.g.*, Logothetis et al., 2001). It is presumed that when some neurons of the brain are active, they consume more oxygen, which further increases blood flow to those specific areas. The detection of blood oxygenation level dependent (BOLD) contrast with MRI (Ogawa et al., 1992) relies on the differences in magnetic properties of oxyhemoglobin (diamagnetic) and deoxyhemoglobin (paramagnetic). As neuronal activation occurs, blood oxygenation increases in nearby capillaries, leading to the decreased concentration of deoxyhemoglobin. Unlike oxyhemoglobin, the paramagnetic deoxyhemoglobin changes the local magnetic field and thus affects T_2- and T_2^*-weighted images. Therefore, the signal is strongly influenced by the oxygenation state of blood. Even though the relationship between the fMRI signal (hemodynamic response) and the underlying neuronal activity is not precisely known, the relation of these activities is indisputable.

The functional activation localization of BOLD fMRI is based on the relative signal changes between the different experimental conditions and on the statistical validation of these changes. Normally, the experiment is an alternating rest and activity stimulation period in a simple box-car design although also event-related fMRI designs can be used (*e.g.*, Dale, 1999). The resulting statistical parametric maps of fMRI signals are overlaid on the corresponding anatomical magnetic resonance (MR) images to show the exact locations of the activations.

Functional MRI is performed with the same device as the MRI. As several images need to be acquired in rapid succession, the overall resolution of the images is greatly reduced from the full potential of the high-end scanners. The most prominent virtue of fMRI is its good spatial resolution while temporal resolution is limited. In these studies, the term fMRI is used to describe the hemodynamic BOLD changes associated with neural activations even though the term fMRI could mean any other nuclear magnetic resonance –based functional imaging method, such as perfusion and diffusion tensor imaging (see, *e.g.*, Huettel et al., 2004, for details on these methods).

2.2.3 Magnetoencephalography

The human brain is composed of approximately 10^{11} *neurons* (*e.g.*, Kandel et al., 2000). When the brain is active the neurons transmit information *via* axons in

action potentials to be transmitted to postsynaptic neurons. Most of the currents visible in external *magnetic fields* are generated by synchronous postsynaptic potentials of cortical pyramidal neurons (*e.g.*, Dale and Sereno, 1993; Okada et al., 1997). However, as the current flow in one single cell is very low, typically 10^4 to 10^5, neurons need to fire simultaneously for the magnetic fields (or electric potentials) to be detected outside the head (*e.g.*, Vrba and Robinson, 2001).

MEG (*e.g.*, Cohen, 1968, 1972; Hämäläinen et al., 1993; Ilmoniemi, 1994; Baillet et al., 2001) measures these fields that are generated by activations of relatively large, yet spatially localized, cortical neuronal populations. There are some sources that are magnetically silent limiting the capabilities of MEG. For instance, a radially oriented current source inside a spherically symmetric conductor does not produce any external magnetic fields, leading MEG to be most sensitive to sources tangential to the head. MEG is poor in detecting sources in the deeper structures of the brain, partially because the magnitude of magnetic field decreases rapidly as a function of distance. Fortunately, much of the cortex is located in the fissures and thus oriented tangentially and close to the scalp.

One of the virtues of MEG is that it provides millisecond scale temporal resolution and with excellent conditions also a spatial resolution of few millimeters. In practice, with two (or more) simultaneously active and neighboring sources, the spatial resolution allows separation of sources which are at the distance of approximately 1 cm from each other. In many situations, different sources are within this range, making the separation task difficult.

MEG is usually measured in a magnetically shielded room as the MEG signals are about a factor of 1 million to 1 billion times smaller than urban magnetic noise. The only practical device for measuring such small biomagnetic signals is the *superconducting quantum interference device* (*e.g.*, Zimmerman, 1977), necessitating the MEG sensors to be placed inside a cryogenic Dewar vessel containing liquid helium (*e.g.*, Cohen et al., 1970; Cohen, 1972; Hämäläinen et al., 1993; Ilmoniemi, 1994).

EEG (*e.g.*, Niedermeyer and Silva, 1999) is a method in which, instead of the magnetic fields, electric potentials are measured. In addition to complementary measurements, it provides information not visible in MEG. EEG is sensitive to all orientations of the sources and also to deep sources. Unfortunately, skull and scalp cause attenuation and smearing to the measured potentials complicating the estimation of the sources. Importantly, EEG can be measured simultaneously with MEG.

2.3 Electromagnetic inverse problem

The core of this thesis is to apply computational methods in solving the *electromagnetic inverse problem*. However, before considering the inverse problem it-

self, the term *forward model* (*e.g.*, Mosher et al., 1999) needs to be clarified. Forward model is composed of solving the electromagnetic fields and potentials generated by the underlying source currents. This relation is governed by Maxwell's equations and in MEG it is readily solved under the *quasistatic approximation* (*e.g.*, Hämäläinen et al., 1993; Ilmoniemi, 1994). In this, the time derivatives in the calculation of magnetic fields can be neglected due to most of the cellular electrical phenomena containing frequencies below 1 kHz. Magnetization of the tissue can also be left out in the considerations. The solution to the forward model is affected by different tissue properties, such as conductivities of the skull and brain, which are in general anisotropic. With MEG signals, a model in which the realistically shaped cranial volume has uniform electrical conductivity and the skull is considered as a perfect insulator is sufficient for many practical purposes (Hämäläinen and Sarvas, 1989; Mosher et al., 1999). Such a single-layer boundary-element model (BEM) is assumed throughout this thesis. In EEG forward computations, three-layer BEM is needed with varying electric properties for the skin, skull, and brain compartments. Otherwise significant errors can be encountered in the source localization procedure (*e.g.*, Ollikainen et al., 1999).

Unfortunately, localizing the source currents based only on the electromagnetic fields outside the head (*i.e.*, the electromagnetic inverse problem) is an ill-posed problem and does not have a unique solution. This is due to the fact that there may be an infinite number of magnetically silent sources producing no detectable fields outside the head (*e.g.*, Sarvas, 1987). Addition of these silent sources do not alter the measured magnetic fields and, thus, finding the one correct solution among many becomes impossible.

Beacuse of the nonuniqueness of the inverse problem, it is always necessary to introduce additional information or assumptions to limit the set of possible solutions. Often, the methods used in tackling the electromagnetic inverse problem are divided into *equivalent current dipole* modeling and *distributed current source* estimation. Both techniques are used, so that Publications I, II, and III involve distributed source estimation whereas Publications IV and V deal with dipolar current sources. Additionally, combining information from different brain imaging methods, MEG and MRI/fMRI in this work, alleviates some ambiguities in estimating neuronal currents in the brain. Throughout the thesis, the electromagnetic inverse problem is treated in Bayesian fashion.

2.3.1 Equivalent current dipole modeling

MEG field patterns are often assumed to be generated by dipolar current sources located in the cortex directly beneath the scalp (*e.g.*, Brenner et al., 1978; Reite et al., 1978; Hari et al., 1980). This assumption employs the ECD model or *dipole fitting* to the MEG inverse problem (*e.g.*, Mosher et al., 1992; Hämäläinen et al., 1993; Baillet et al., 2001). In ECD modeling, one assumes that the ex-

tents of activated areas are small enough to be truthfully represented by a set of point-like current dipoles. By using automatic or manually guided optimization methods, the ECD model giving the best fit to the measured data is obtained. The method is usually applied to stimulus-locked responses of time-domain measurements although frequency-domain analysis is also feasible (*e.g.*, Lütkenhöner, 1992; Salmelin and Hämäläinen, 1995). In MEG, these so-called *evoked fields* (EF) are obtained by averaging the waveforms that are recorded while presenting repetitions of the same physical stimulus to the subject. The corresponding concept in EEG is called an evoked potential.

Typically, the estimated ECD is overlaid on the high-resolution MR images to reveal the locations of the corresponding currents in individual cortical areas. In dipole fitting, user expertise and partly heuristic methods are required to obtain good solutions. For example, if an automatic fitting algorithm places a dipole outside the cortical gray matter, manual intervention is needed as there are no current sources in the white matter or outside cortex. With multiple dipoles, ECD modeling requires approximate and manual techniques as the related optimization problem becomes insolvable. A major problem with existing methods is that the number of dipoles need to be determined *a priori* to optimization.

In many cases the ECD model is an adequate assumption. However, the actual cortical activation patterns visible in MEG are generally presumed to be elicited by a large number of neurons (*e.g.*, Okada et al., 1997; Vrba and Robinson, 2001) extending over few square centimeters of gray matter. With dipolar sources, the accurate modeling of such current distributions on the cortex is difficult if not impossible.

2.3.2 Distributed current source estimation

In distributed inverse estimates, every point in the source space is often thought to contain a small dipolar source along with some minimum-norm (*e.g.*, Hämäläinen and Ilmoniemi, 1984, 1994; Matsuura and Okabe, 1995, 1997) or maximal smoothness (*e.g.*, Pascual-Marqui, 2002) properties for the currents. At present, the discretized source space is generally a realistic cortical surface or volume, although spherical source space models are still used due to simple and fast implementation.

Perhaps the best-known distributed approach is the *minimum-norm estimate* (MNE), in which a shortest source current vector (in the mathematical ℓ^2-norm sense) explaining the data is estimated (Hämäläinen and Ilmoniemi, 1984, 1994). Although different variations of the conventional MNE have been widely used previously (*e.g.*, Clarke, 1989; Ioannides et al., 1990; Wang et al., 1992; Dale and Sereno, 1993; Dale et al., 2000; Hauk, 2004) some undesirable characteristics remain with the solutions from the viewpoint of an empirical neuroscientist interpreting the results. The estimates are rather diffuse and localized sources are

biased towards the surface of the cortex.

With the minimum-current estimate (MCE) (Uutela et al., 1999), an ℓ^1-norm constraint (*e.g.*, Matsuura and Okabe, 1995, 1997; Beucker and Schlitt, 1996; Bücker et al., 2001) is imposed on the currents instead of the Euclidean norm, yielding inverse estimates that are more focal than with MNE. Depth weighting (*e.g.*, Köhler et al., 1996; Lin et al., 2006b) has been proposed to improve the localization of deep sources. Several other modifications to the minimum-norm estimate have been suggested, such as restricting the orientation and location of the current source in each distributed point in the source space, to be perpendicular (*e.g.*, Dale and Sereno, 1993, with ℓ^2) or almost perpendicular (*e.g.*, Lin et al., 2006a, with ℓ^1 and ℓ^2) to the cortical mantle. These methods require individual cortical reconstructions based on the anatomical MR images. With strict cortical constraints the source space reconstructions, and thus also the MRI data, need to be of an exquisite quality.

2.3.3 Combination of different imaging modalities

Imaging modalities are commonly combined by using anatomical MR images in MEG/EEG source estimation. Volumetric and surface reconstructions are routinely used to constrain the possible source locations and orientations with distributed source imaging methods (*e.g.*, Dale and Sereno, 1993), for instance. Furthermore, with dipole fitting methods, the dipole locations are generally displayed on the anatomical images, and the individual reconstructions can be used to create more realistic forward models instead of spherical symmetry.

As many modern MEG devices also facilitate the simultaneous recording of EEG, there is increasing interest to the combination of EEG and MEG in solving the electromagnetic inverse problem. Previously, it has been shown that combined EEG/MEG measurements give the best results to the source localization problem (*e.g.*, Baillet et al., 1999; Liu et al., 2002) but there is still some uncertainty how these methods should be combined. In the present study EEG data is not used, but in principle it is rather straightforward to take it into account in the models.

Functional MRI information has been incorporated to the minimum-norm estimation, for example, by using it to adjust the source variance parameters (Liu et al., 1998; Dale et al., 2000), or by guiding the MEG source estimate by minimizing a distance to a subspace defined by fMRI data (Ahlfors and Simpson, 2004). The MEG/EEG inverse algorithm can also be seeded with locations from the fMRI data or the separate results can be directly compared with no obvious mathematical integrative model (*e.g.*, Ahlfors et al., 1999). As the exact relationship between the electric currents and the hemodynamic response is still unknown, the pursuit of the physiologically "correct" way of combining MEG and fMRI stays in motion.

2.3.4 Bayesian formulation to the MEG inverse problem

In neuroimaging, Bayesian formulation has been used in describing the electromagnetic inverse problem. Several different methodologies based on, for instance, anatomical, physiological, and temporal information have been proposed (*e.g.*, Dale and Sereno, 1993; Phillips et al., 1997; Baillet and Garnero, 1997; Liu et al., 2002; Phillips et al., 2002a,b; Sato et al., 2004; Phillips et al., 2005). A Bayesian perspective to the MEG inverse problem is especially convenient with the distributed inverse models. In the following, a brief generic Bayesian formulation to the MEG inverse problem is presented to give an overview of the methodology and concepts involved in this thesis.

In MEG, the solution to the forward problem yields a linear relationship between the time-dependent source currents $\mathbf{s}(t)$ and measured signals $\mathbf{b}(t)$

$$\mathbf{b}(t) = \mathbf{A}\mathbf{s}(t) + \mathbf{n}(t), \tag{2.8}$$

where $\mathbf{n}(t)$ is the measurement noise vector and $\mathbf{A}$ is the gain matrix where each column gives the measured signal distribution for one dipolar current located on the source space. Additive Gaussian measurement noise is often assumed, leading to a linear regression model described in statistical terms as

$$p\big(\mathbf{b}(t)|\mathbf{s}(t), \mathbf{C}, \mathcal{M}\big) = \frac{1}{\sqrt{|\mathbf{C}|(2\pi)^M}} \cdot \mathrm{e}^{-\frac{1}{2}\left(\mathbf{b}(t)-\mathbf{A}\mathbf{s}(t)\right)^{\mathrm{T}}\mathbf{C}^{-1}\left(\mathbf{b}(t)-\mathbf{A}\mathbf{s}(t)\right)}, \tag{2.9}$$

where $\mathbf{C}$ is the noise covariance, M the number of measurement sensors, and $\mathcal{M}$ the implicit and explicit modeling assumptions, such as Gaussian noise, cortical constraints, utilized conductivity values, selected time windows, and so forth, all affecting various parts of the model. This probabilistic expression for the observational model corresponds to the likelihood function in Eq. 2.3.

The statistical prior properties of the source currents can be described by an exponential density

$$p_0\big(\mathbf{s}(t)|\mathcal{M}\big) = \frac{1}{\alpha} \cdot \mathrm{e}^{-\beta f(\mathbf{s}(t))}, \tag{2.10}$$

where α and β are constants and $f(\cdot)$ is a function of the unknown source currents $\mathbf{s}(t)$. This representation encompasses, for example, the multivariate Gaussian models (Baillet et al., 2001).

In case of fixed data and numerical considerations, the normalization term $p\big(\mathbf{b}(t)|\mathcal{M}\big)$ can be omitted (see, Eq. 2.3 on page 3) and the posterior distribution is directly proportional to the product of the likelihood and the prior for the source currents

$$p\big(\mathbf{s}(t)|\mathbf{b}(t), \mathcal{M}\big) \propto p\big(\mathbf{b}(t)|\mathbf{s}(t), \mathcal{M}\big) \cdot p_0\big(\mathbf{s}(t)|\mathcal{M}\big). \tag{2.11}$$

It is straightforward to insert different parameter representations or additional variables to the model and assign suitable prior densities to them according to

prior beliefs. Maximization of Eq. 2.11 leads to the MAP estimate, whereas numerical methods are needed for approximating complicated posterior distributions. In the MCMC sampling of the posterior distribution, or estimation of the parameter values of $\mathbf{s}(t)$ in this generalized example, the log-posterior is considered for computational purposes

$$\log\Big(p\big(\mathbf{s}(t)|\mathbf{b}(t),\mathcal{M}\big)\Big) \propto \log\Big(p\big(\mathbf{b}(t)|\mathbf{s}(t),\mathcal{M}\big)\Big) + \log\Big(p_0\big(\mathbf{s}(t)|\mathcal{M}\big)\Big). \quad (2.12)$$

Desired parameter estimates can be made based on the resulting MCMC samples that represent the posterior distribution.

In case of conventional MNE (in the presented formalism), the ℓ^2-norm for the source currents is represented by a Gaussian prior distribution with fixed covariance matrix. The maximization of the resulting log-posterior corresponds to the minimization of the associated error function. This yields the traditional linear inverse operators in a Bayesian way (*e.g.*, Dale et al., 2000; Phillips et al., 2002a). In minimum-norm estimation, the choice of using the ℓ^2-norm prior is often made by the researcher and the produced inverse estimates may be argued to be (physiologically) overly smooth due to the mathematical *a priori* assumption.

Recently, Sato et al. (2004) introduced a hierarchical generalization to the minimum-norm estimation. Each source space point is assumed to have its own variance parameter instead of one parameter value for all. These variances are inferred from the data using an automatic relevance determination prior (*e.g.*, Neal, 1996). This leads to a more focal solution in which the data are essentially explained by a few prominent source space locations whereas other locations are dampened by the prior. The approach is nonlinear, hence variational Bayesian method was applied to approximate the posterior distribution.

Some parametric dipole fitting or extended region models (*e.g.*, Schmidt et al., 1999; Bertrand et al., 2001a,b; Kincses et al., 2003; Jun et al., 2005, 2006) are analyzed with numerical MCMC methods, so that the full posterior probability distribution can be evaluated instead of just one maximum *a posteriori* estimate. The feasibility of obtaining a large number of likely solutions to the MEG inverse problem, rather than one single estimate, was first demonstrated by Schmidt et al. (1999) with an active region model consisting of number, location, and extent of active brain areas. Later, they extended their analysis to the full spatiotemporal MEG/EEG data set (Schmidt et al., 2000). The most natural way of numerically sampling the number of active regions or dipoles is done using reversible jump MCMC (Green, 1995). This has been used previously (*e.g.*, Bertrand et al., 2001a,b; Jun et al., 2005) and also combined to parallel tempering methods which are used to evade local convergence (Bertrand et al., 2001a,b).

In recent work by Jun et al. (2005), instead of extended regions (*e.g.*, Schmidt et al., 1999; Kincses et al., 2003), spatiotemporal Bayesian inference dipole analysis for MEG was proposed. Their model is shown to be faster than the extended

region model, and it does not require the use of individual anatomical information or any prior knowledge about the number of underlying dipoles. Additionally, they marginalize over the given background noise considering it as an uncertain parameter. Lately, they improved their model to contain active time range information, which allows the source constellation to change over time (Jun et al., 2006). In this, additional parameters of activation starting and ending timepoints for each source are also inferred by MCMC sampling.

2.4 On human cortical processes

The human brain is the most complicated organ in our body and with connections to nervous, sensory, and muscular systems, it guides our functioning (*e.g.*, Kandel et al., 2000). Only a brief description of the anatomy and operation of (primary) auditory, visual, and somatomotor cortices is given, enough to understand the experiments performed in this study.

Motor cortices can be roughly divided into *primary motor cortex* (M1) and premotor areas (supplementary motor cortex and premotor cortex). Primary motor cortex is located in the precentral gyrus (Fig. 2.3) in both cerebral hemispheres and organized according to so-called homuncular representation in which specific muscles are governed by different regions in M1. Important parts of the body, such as the face and fingers, hold the largest areas of M1. The supplementary motor cortex is situated medially in front of M1 in the frontal lobe and premotor cortex laterally from the former. M1 is active in planning and execution of movements while the premotor areas are active only during the preparation of movement. Motor tasks require constant fine adjustment and, thus, there is clear functional connectivity between primary motor and *primary somatosensory areas* (S1). The postcentral gyrus is associated with the primary somatosensory information processing and it is organized in similar manner to M1. Motor control and sensory pathways between the brain and the rest of the body are crossed. Therefore, operation of the left hand, for example, is controlled *contralaterally* by the right hemisphere (RH) and vice versa, although *ipsilateral* connections, that is, left hemisphere (LH) controlling the left hand, exist.

The *primary auditory cortex* (A1) is located in both hemispheres in the temporal lobe in the posterior half of the superior temporal gyrus extending to Sylvian fissure as Heschl's gyrus. Auditory evoked fields have been extensively studied and localized with ECD models in the literature (*e.g.*, Reite et al., 1978; Farrell et al., 1980; Hari et al., 1980). Typically, any auditory stimulus or change in a continuous sound evokes a response whose cortical location depends of the stimulus properties. One such property is the frequency of the presented stimulus (see, Romani et al., 1982, for tonotopic organization of the primary auditory cortex). The most prominent component of the EF is the N100m that peaks about 100 ms after

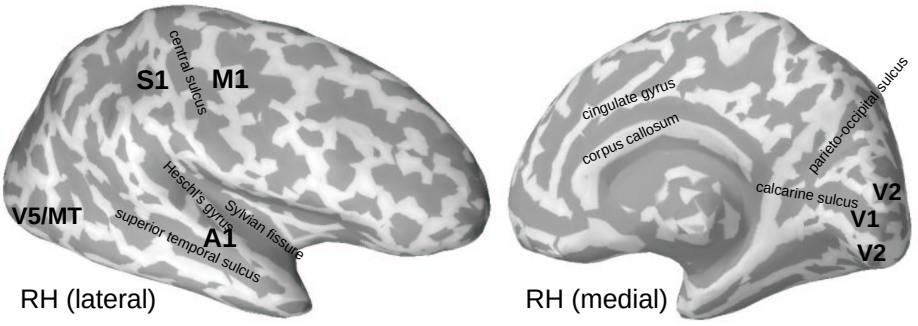

Figure 2.3: Approximate primary cortical areas and major anatomical landmarks are indicated on lateral and medial view of the inflated right hemisphere to facilitate interpretation and comparison to the corresponding images in the publications.

the stimulus. Together with the other components, such as early N19m and late P200m, they are of cortical origin (see, *e.g.*, Hämäläinen et al., 1993; Ilmoniemi, 1994, for more).

The visual cortex is generally divided into *primary visual cortex* (*i.e.*, striate cortex or V1) and *extrastriate visual areas* that include the areas V2, V3/VP, and V5/MT. V1 is located in the occipital lobe around and in the calcarine sulcus. The ventral stream ("what pathway") goes from V1 to V2 and onwards to the inferior temporal lobe and is considered to be associated with object and form representations in the cortex. The dorsal stream ("where pathway") is associated with object locations and motion along with the control of eyes and arms when visual information processing is involved. The dorsal stream goes through V2 to V5/MT and onwards to the inferior parietal lobe. Visually evoked fields (*e.g.*, Brenner et al., 1975; Teyler et al., 1975) measured in MEG have been used to study the *retinotopic* organization of V1. The first results showed that information from left visual field go to the right hemisphere and vice versa. Since the development of fMRI (*e.g.*, Ogawa et al., 1992; Kwong et al., 1992; Belliveau et al., 1991) the representations of the visual fields in human cerebral cortex (*e.g.*, DeYoe et al., 1996) and mappings of borders and sizes of human retinotopic visual areas (*e.g.*, Sereno et al., 1995; Dougherty et al., 2003) have become more accurate. Traditionally, flickering checkerboard stimuli of certain spatial and temporal frequency have been used as they are known for producing a good response in V1 (*e.g.*, Engel et al., 1997). Functional imaging has also been used to study the visual areas with operational specialization, and, for instance, V5/MT is known to be sensitive to visual motion.

Accumulating evidence exists that the human visual system is anatomically

and functionally organized not only for bottom-up hierarchical processing but also for top-down modulation with higher cognitive tasks (*e.g.*, Courtney and Ungerleider, 1997). For scrutinizing such complicated cortical networks, the analysis methods need to be capable of high accuracy in both spatial and temporal domain.

Audiovisual integration is used to describe the processes in the brain that combine the information from these two different processing streams. For instance, seeing articulatory movements of a speaker's face significantly improves the perception and speech comprehension especially in noisy conditions. Audiovisual or some other form of crossmodal integration is affected by several other processes, such as the focus of the perceiver's attention or stimulus characteristics. In this thesis, the utilized sensory stimuli (*i.e.*, auditory, visual, and motor task) are mainly unisensory, so that no notable integrative processes are presumed to take place. However, with more complicated multisensory stimulation this assumption is unjustifiable.

Chapter 3

Aims of the study

The overall aim of this study was to create new and improve existing state-of-the-art computational methods for solving the MEG inverse problem. The main objective was to utilize the individual anatomical and functional magnetic resonance imaging data of the participants, keeping in mind that the models should be feasible in real neuroscientific investigations. Our guideline was to utilize Bayesian inference in order to be able to examine the whole distribution of different solutions rather than one single point estimate.

Specifically, Publication I was motivated by the Bayesian interpretation of the electromagnetic inverse problem. We aimed at determining whether there is enough information in the data to determine which ℓ^p-norm order p together with the least squares error function of the data gives rise to the best solutions.

In Publication II, we wanted to compare the results of a full Bayesian analysis via MCMC sampling to a newly introduced variational Bayesian method with a hierarchical generalization of the traditional MNE (Sato et al., 2004). The objective in Publication III, was to test the hierarchical VB model for the first time with empirical data and discuss practicalities in using the method.

We wanted to alleviate the computationally heavy process of MCMC sampling and decided to reduce the dimensionality of the parameter space by reformulating the problem with dipolar sources in Publication IV. We aimed at improving a recently published similar model (Jun et al., 2005) by utilizing cortical location and orientation constraints known to be useful in the source estimation task. In Publication V, the goal was to introduce a novel way of including fMRI data to the MCMC based MEG inverse modeling and show that it improves the performance of the sampling method.

Chapter 4

Overview of the experimental measures

4.1 Data simulations

In all the publications, simulated MEG data were generated using a single-layer boundary-element model assuming the skull to be a perfect insulator and the cranial volume to have homogeneous electrical conductivity. The forward model and the gain matrix were computed using the MNE software[1] developed at Athinoula A. Martinos Center for Biomedical Imaging, Massachusetts General Hospital, Charlestown, MA, USA.

Importantly, in inverse estimation, the term *inverse crime* is used to describe all those elements that are fixed in the forward model construction and later presumed known in the solution part. It is common within MEG inverse problem simulations that the estimation is done using the same gain matrix that was used for data simulation. In this thesis, different grid discretizations were always employed for simulation and estimation in order to avoid the most common type of inverse crime. Different discretizations were used in the analysis phase for studying the effect of grid discretization size to the solutions.

In Publication I, the signal-to-noise ratio and extents of the simulated sources were varied and random zero-mean Gaussian noise was added to the simulated measurements. In Publication II, the simulated data were similar with additive Gaussian measurement noise, but contained several timepoints instead of spatial-only data as in Publication I. The locations of the sources were manually chosen to correspond to plausible physiological cortical patches in both publications.

In Publications IV and V, realistic measurement noise was added to the simulated fields prior to averaging in order to produce the same spatiotemporal noise structure as with empirical data. The locations and latencies of the simulated

[1] URL: http://www.nmr.mgh.harvard.edu/martinos/userInfo/data/sofMNE.php

sources were chosen manually to be similar to their empirical equivalents. In addition, simulated fMRI data were created by placing Gaussian kernels on the source space enveloping the desired sites of activation in Publication V.

4.2 Empirical data

Three different categories of empirical MEG data were acquired throughout the study. MEG data were analyzed for a self-paced somatomotor finger-lifting task (Publication I), simple auditory tone presentation (Publications III and IV), and two types of visual stimulation (Publications III, IV, and V). Empirical fMRI data were acquired for the visual stimulation in Publication V, whereas anatomical MR images were acquired for all participants of the experiments in order to obtain the individual source space reconstructions for the analyses. For the calculation of the forward model, the MNE software was employed.

4.2.1 MEG data

MEG data were acquired in a magnetically shielded room with a Vectorview MEG system (Elekta Neuromag Oy, Helsinki, Finland) located at Low Temperature Laboratory, Helsinki University of Technology. Voluntary subjects participated to the experiments. In addition to the MEG, bipolar electro-oculogram was obtained in all of the measurements and later used for eye-blink artifact removal. The sensor array of the system used is composed of 306 MEG channels arranged in triplets of two orthogonal planar gradiometers and a magnetometer at 102 locations, measuring the magnetic field gradient and the magnetic field, respectively (Fig. 4.1). All preprocessing of MEG data were performed using inhouse designed functions for MATLAB (The MathWorks, Inc., Natick, Massachusetts, USA), Vectorview MEG system software, and Neuromag FIFF-file access functions[2].

4.2.2 MRI and fMRI data

High-resolution T_1-weighted three-dimensional anatomical MR images were obtained with a 3 T scanner (General Electric Signa, Milwaukee, Wisconsin, USA) located at Advanced Magnetic Imaging Centre, Helsinki University of Technology. The anatomical MR images of two subjects were scanned with 1.5 T scanners (Siemens Sonata and Vision, Erlangen, Germany) located at Massachusetts General Hospital, USA and Helsinki University Central Hospital, Finland. The local 3 T scanner was used for acquiring the fMRI images depicting BOLD contrast in Publication V.

[2] URL: http://www.kolumbus.fi/kuutela/programs/meg-_pd/

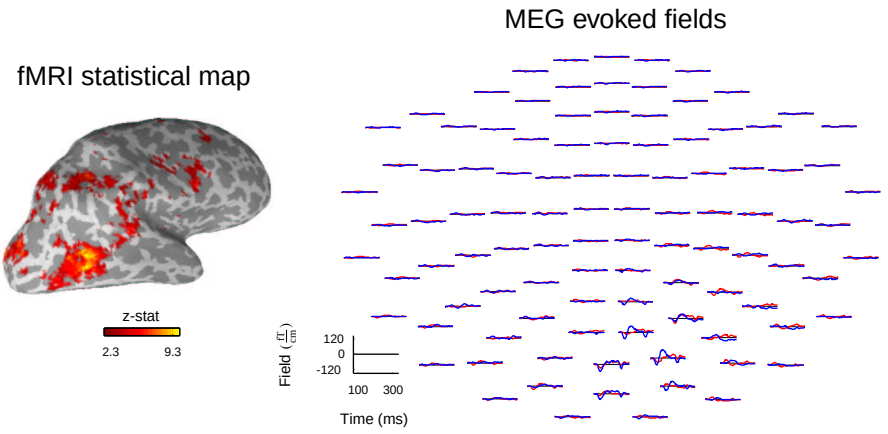

Figure 4.1: Functional MRI and MEG data of presenting visual lower left quadrant drifting grating stimulus to a subject. Statistical parametric map of fMRI data on inflated right hemisphere depicts the BOLD contrast, whereas the waveforms of the MEG evoked fields show the two orthogonal magnetic field gradients. The MEG channels are viewed from the top, nose of the subject pointing up in the figure.

Preprocessing of the anatomical MRI data sets were performed with the Freesurfer software[3] also developed at Athinoula A. Martinos Center for Biomedical Imaging. An automated segmentation algorithm was used to obtain the geometry of the white-gray matter boundary (see, Dale et al., 1999; Fischl et al., 1999, 2001, for details). This limited the locations and orientations of the possible source currents based on the assumption that most of the currents visible to MEG are produced in the cortical pyramidal neurons. This information was applied in the forward BEM calculations. Inflation of the cortical layers (Fig. 4.2) was performed using Freesurfer. For further processing and visualization, the brain surfaces were transformed into MATLAB.

Functional MRI analyses in Publication V were conducted using the FSL software tools (see, Smith et al., 2004, for details and additional information) developed at Oxford Centre for Functional Magnetic Resonance Imaging of the Brain, Department of Clinical Neurology, Oxford University, UK.

4.3 Analysis environment and visualization

Excluding the preprocessing procedures described previously in this chapter, all other preprocessing of MEG data, numerical analyses, and visualization were per-

[3]URL: http://www.nmr.mgh.harvard.edu/martinos/userInfo/data/sofFreeSurf.php

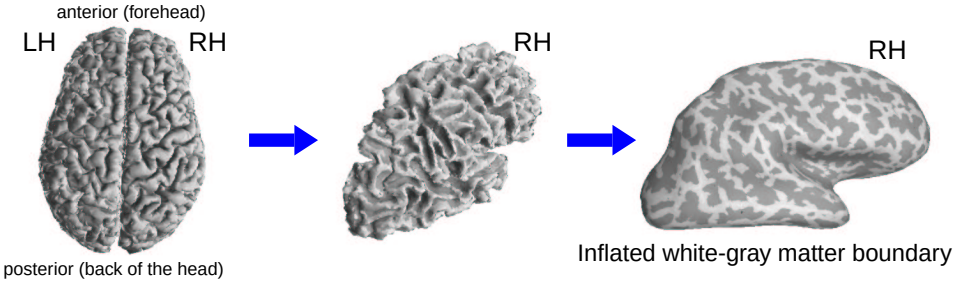

Figure 4.2: In the inflation process, the white-gray matter boundary is extracted and inflated to reveal the sulci and gyri of the cortex.

formed using MATLAB. A set of MATLAB functions used to import, preprocess, and analyze the data was written. Preprocessing of MEG data includes filtering, averaging, artifact removal, noise covariance estimation, and model-specific initializations. With fMRI data, only the model-specific initializations were needed as statistical analyses were done using different software.

For the numerical analyses, appropriately designed and tailored sampling schemes were written. One of the sampling methods used (*i.e.*, slice sampling) was written to a more general form and included in a collection of MATLAB functions for Bayesian inference with MCMC methods[4] developed and distributed at Laboratory of Computational Engineering, Helsinki University of Technology. Many of the functions available in the toolbox were used as such.

MATLAB functions were also created for visualizing the results. The tools are capable of displaying cortical surfaces and overlaying activations and curvature information to them. Realistic individual white-gray matter boundary surfaces were used in the analyses while the inflated cortical mantles were exploited for visualization purposes. All the images in the publications and thesis were produced in MATLAB using these functions with data-specific modifications.

The preprocessing, numerical analyses, and visualizations were mostly performed with ordinary Linux workstations (Pentium III/4, 1–3.2 GHz processor, 1024–4096 MB of RAM). The code was optimized for MATLAB to keep computing time reasonable although in some cases special actions were needed in dividing the computer runs to a large cluster of Linuxes for achieving results faster. Stand-alone C language compilations of the MATLAB code were also generally used.

[4] URL: http://www.lce.hut.fi/research/mm/mcmcstuff/

Chapter 5

Overview of the models

In this chapter, main features and results of the analyses with the models are summarized. Details can be found in the corresponding publications. A general discussion and description of possible future work are included at the end.

5.1 Publication I: ℓ^p-norm model

5.1.1 Introduction

In the Bayesian interpretation of the minimum-norm and minimum-current estimates, prior information of the current distribution is embedded to the model as mathematical ℓ^2- and ℓ^1-norm constraints, respectively. The choice of the ℓ^p-norm order p leads to either focal ($p = 1$) or rather diffuse ($p = 2$) estimates, although any value between 1 and 2 could be used. In Publication I, we circumvent this choice by trying to infer p from the data. We assume the noise covariance $\mathbf{C}$ to be diagonal and known up to a scaling constant σ_l in order to evade the computationally heavy sampling of $\mathbf{C}$. For additional computational convenience, we whiten the model-specific gain matrix and measured fields $\mathbf{b}$ by multiplying them with $\mathbf{C}^{-1/2}$. Although being a spatial-only study, temporal structure could be added with the cost of computational time.

In the preliminary sampling runs, correlations between the ℓ^p-norm prior width and source current parameters $\mathbf{s}$ were present. Thus, we reparametrized the prior structure yielding a hyperparameter β that defines the ℓ^p-norm order, so that

$$p = \frac{2}{1+\beta}, \tag{5.1}$$

and the prior itself is as in Box and Tiao (1973, see, Ch. 3.2.1). The parameter value $\beta = 1$ corresponds to the ℓ^1-norm model and $\beta = 0$ to the ℓ^2-norm model. In Bayesian data analysis, our choice of uniform prior for β might have an effect on the implicit prior of p, also noted by one of the anonymous referees, so that

the model would slightly favor values of p close to 1 over the values close to 2. However, we performed a prior sensitivity analysis for β, and showed that the effect of implicit prior propagating to the shape of the posterior distribution was insignificant considering our conclusions.

Collecting the pieces of our ℓ^p-norm model, we arrive at an unnormalized parameter posterior density of

$$p(\mathbf{s}, \sigma_l, \sigma_c, \beta|\mathbf{b}) \propto p(\mathbf{b}|\mathbf{s}, \sigma_l) \cdot p(\sigma_l) \cdot p_0(\mathbf{s}|\sigma_c, \beta) \cdot p(\sigma_c) \cdot p(\beta), \tag{5.2}$$

where priors for noise-scale parameter σ_l, current prior width σ_c, and β are assumed uniform. The likelihood of the data is of the presented general form without time dependency and with diagonal $\mathbf{C}$ (see, Eq. 2.9 on page 16).

The posterior distribution was numerically sampled with slice sampling and the convergence of several Markov chains was monitored visually and by using the potential scale reduction factor. Posterior predictive sampling was employed in obtaining a measure between different ℓ^p-norm models with respect to the grid discretization size and of comparison between the ℓ^1-, ℓ^2-, and ℓ^p-norm models (Fig. 5.1). The model was tested with empirical MEG data of an active finger-lifting task and with simulations having varying source extents and SNRs.

5.1.2 Results

With the data presented in the publication, our model favors values of the ℓ^p-norm order p close to 1, yielding more focal solutions than the traditional minimum-norm estimation. However, the shapes of the posterior distributions of p (histograms) are clearly dependent of the underlying simulated source configuration, used grid discretization, and SNR. Based on the qualitative results and the posterior predictive sampling, the optimal grid discretization size for our model is around approximately 3500 points for the whole cortical surface of both hemispheres. With poorer SNR, the distribution of p gets flatter, suggesting that inferring p from the data is more difficult with increasing noise. Wider and deeper simulated source configurations seem to localize as more diffuse activations on the cortex than the focal superficial ones.

With the empirical data, predicted data fits are reasonable and the posterior distribution of p suggests the use of ℓ^1-norm for the currents, although the solutions are moderately spread. Lifting of the right index finger yields spatial activation contralaterally to the hand area of M1 and S1. Left index finger-lifting task in turn generates activity to the right hemisphere (Fig. 5.2). This is in agreement with the literature.

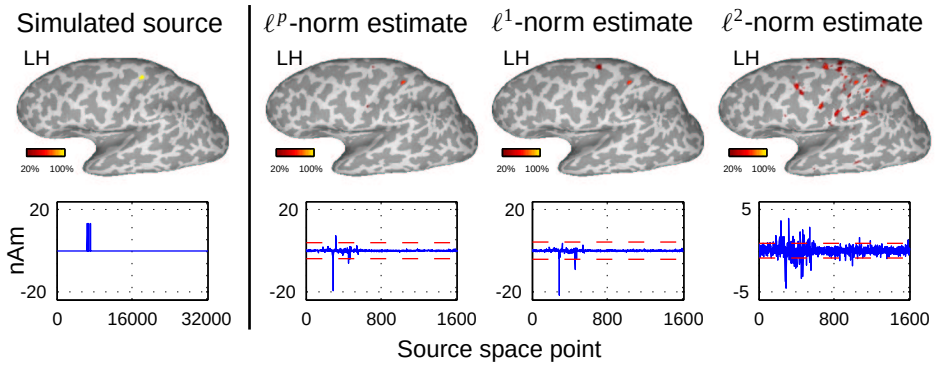

Figure 5.1: Comparison of different ℓ^p-norm solutions obtained with MCMC sampling. The estimates are interpolated on the original dense grid for visualization purposes. Only the absolute values exceeding 20% of the maximum absolute amplitude of the estimate are plotted on the inflated brain.

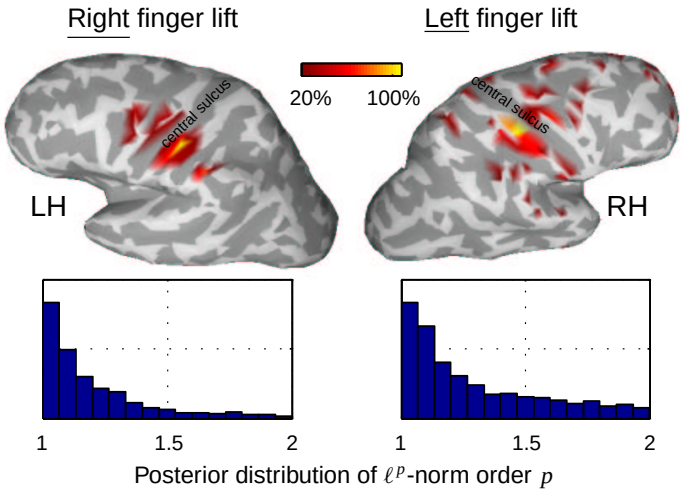

Figure 5.2: Inverse estimates and posterior distribution of p of the empirical index finger lifting task.

5.2 Publications II and III: Hierarchical MNE

5.2.1 Introduction

In Publications II and III, a time-dependent observational model assuming multivariate Gaussian noise independent of time is united with a Gaussian prior distribution for the source current parameters. In this, each cortical source space location is assumed to have its own *precision* (*i.e.*, inverse variance) parameter α_{VB}, so that in contrast to the traditional MNE, the sources $\mathbf{s}(t)$ can have *a posteriori* different variances, that is, some sources are more likely to yield zero amplitude values than others. Furthermore, a hyperprior is imposed for the precision parameters and for the scale parameter β_{VB}, which is included in the calculations to facilitate the variational Bayesian estimation (Sato et al., 2004). The precisions are inferred from the measurement data using automatic relevance determination prior (*e.g.*, Neal, 1996; Sato et al., 2004) on them. In Publication II, inverse solutions with MCMC sampling were compared to those obtained with the VB approach using simulated data, whereas in Publication III, empirical MEG data was analyzed for the first time with the hierarchical variational Bayesian method.

The conditional distributions required for the MCMC sampling scenario with the hierarchical MNE (Publication II), are derived from the full joint probability of the data, parameters, and hyperparameters. Gibbs sampling can be used for

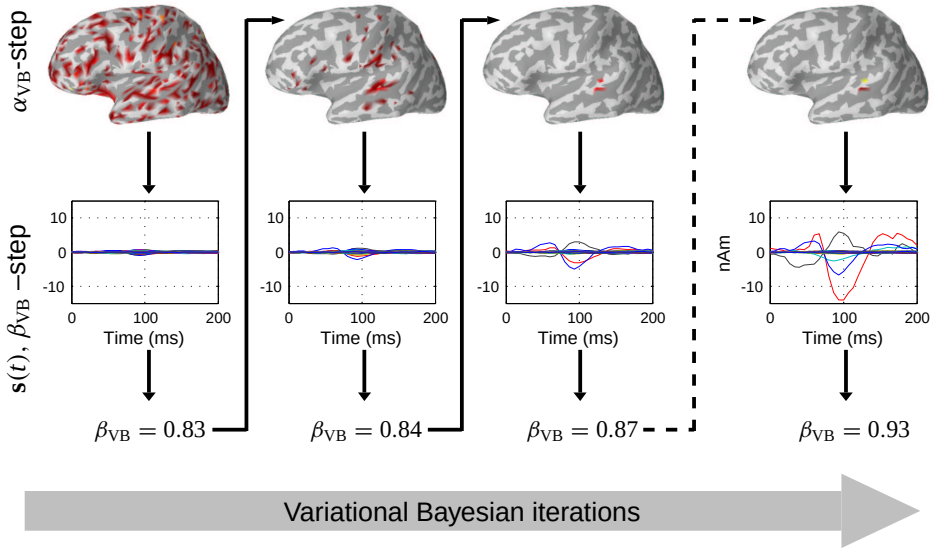

Figure 5.3: Principle of the VB-approach.

sampling all but one of the conditional distributions. For the estimation of this one hyperparameter of the prior, slice sampling is used instead.

In the variational Bayesian framework (Publications II and III), the currents and precisions are assumed to factorize in two parts $q_1\left(\mathbf{s}(t), \beta_{\mathrm{VB}}\right)$ and $q_2\left(\alpha_{\mathrm{VB}}\right)$, and the two q-distributions that maximize the free energy are searched. The algorithm itself is divided into $\mathbf{s}(t)$, β_{VB} –step and α_{VB}-step, for obtaining the solution by successive iterations (Fig. 5.3).

5.2.2 Results

The obtained inverse estimates are evidently more focal than with basic MNE. However, the posterior distribution seems to be multimodal. When compared to each other, MCMC and VB produce similar results although the multimodality of the posterior was more clearly observed in the different MCMC simulations. This could be due to the VB approach having a tendency of converging towards posterior modes containing most of the probability mass. Our results clearly show that the hierarchical MNE model is sensitive to hyperprior selection, although especially the VB method can be used to produce physiologically credible estimates in a rather automated fashion. The empirical data analyzed in Publication III was previously analyzed in Publication IV with a multiple dipole localization method. Both models yielded similar results.

5.3 Publication IV: Cortically constrained analysis of multiple dipoles

5.3.1 Introduction

Conventional dipole fitting methods and algorithms in their basic form require both user expertise and some prior knowledge of the locations or at least the number of underlying current dipoles. In Publication IV, we assumed the notation of a recent spatiotemporal Bayesian dipole inference model (Jun et al., 2005) and implemented a similar model with several modifications. First, instead of a spherical forward model, we employed a more realistic forward model based on the subject's individual anatomy and, second, we restricted the possible source locations to being located and oriented perpendicular to the cortical mantle.

Both data simulations and empirical MEG data were analyzed with the method, the simulated data having exactly the same noise covariance structure than the empirical data. The empirical data sets were acquired in an experiment producing activations to the human auditory and visual systems to see whether this type of automatic dipole fitting methods could be used to study audiovisual processes in the brain. Notably, prior knowledge of the locations and number of underlying sources is not required.

In our sampling scheme, a mixture of three different MCMC methods was constructed. As a new feature, slice sampling was used to sample the location of each specific dipole on the source space of white-gray matter boundary. As the parameter space sampled with slice sampling needs to be continuous, a compact parametrization of the source space grid points with spherical angle coordinates was used. Slice sampling should in principle switch well between different modes and, therefore, perform better than the previously used methods. Standard Metropolis–Hastings was used in switching the hemisphere of a randomly selected dipole and RJMCMC to perform the transdimensional sampling between varying number of dipoles. Our method is initialized with random location on the cortex, whereas the existing algorithms are frequently initialized with a location close to conceivable source locations.

In order to reduce the computational load of our spatiotemporal method, also intended to be used for analyzing long data sets, we speed up the procedure by reducing the dimensionality of the sensor space. This is done by exploiting *singular value decomposition* (SVD) of the (transposed) gain matrix $\mathbf{A}^{\mathrm{T}} = (\mathbf{U}\Lambda\mathbf{V}^{\mathrm{T}})$, where $\mathbf{U}$ and $\mathbf{V}$ are unitary matrices and Λ is a diagonal matrix. Manipulation of the gain matrix $\mathbf{A}$ and the measurements $\mathbf{b}(t)$ lead to

$$\mathbf{A} = \left(\mathbf{U}\Lambda\mathbf{V}^{\mathrm{T}}\right)^{\mathrm{T}} \approx \left(\mathbf{U}_n \cdot \Lambda_n\mathbf{V}^{\mathrm{T}}\right)^{\mathrm{T}} = \mathbf{V}\Lambda_n^{\mathrm{T}} \cdot \mathbf{U}_n^{\mathrm{T}} = \widetilde{\mathbf{A}} \cdot \mathbf{U}_n^{\mathrm{T}} \tag{5.3}$$

$$\mathbf{b}(t) = \mathbf{b}(t) \cdot \mathbf{I} = \mathbf{b}(t) \cdot \mathbf{U}\mathbf{U}^{\mathrm{T}} \approx \mathbf{b}(t)\mathbf{U}_n \cdot \mathbf{U}_n^{\mathrm{T}} = \widetilde{\mathbf{b}}(t) \cdot \mathbf{U}_n^{\mathrm{T}} \tag{5.4}$$

where n is calculated so that the estimates cannot be expected to yield smaller error than the measurement error. $\widetilde{\mathbf{A}} = \mathbf{V}\Lambda_n^{\mathrm{T}}$ and $\widetilde{\mathbf{b}}(t) = \mathbf{b}(t)\mathbf{U}_n$ are the modified gain matrix and linearly independent measurement combinations used in the rest of the model formulation.

Marginalizations of the noise covariance parameter $\mathbf{C}$ and source current time courses $\mathbf{s}(t)$ were conveniently adopted from previous work by Jun et al. (2005) with adaptations made to match our parametrization and SVD speed-up strategy. These steps lead to the final approximated posterior distribution of the dipole number and location parameters. Posterior realizations of the current timecourses can be drawn from a multivariate normal distribution by using the existing samples.

5.3.2 Results

Although the method by Jun et al. (2005) seemed to consistently localize multiple simulated dipoles, our sampling scheme did not perform optimally in the presence of apparently multimodal parameter posterior distribution, partially due to the rigid cortical orientation constraints. It is evident based on our analyses that Markov chains of different data sets converge to a local mode rather quickly. In general, however, it is extremely difficult to determine whether the chains have converged globally as the samples might jump to a different mode after long sta-

tionary sampling in one mode (see, Fig. 2.2c on page 5). Because of these somewhat limited mixing properties especially in the more complex cases (with more than two nearby dipoles), one cannot compare how much probability mass each mode has. This spoils the possibility of Bayesian comparison between the different solution candidates. Thus, it is left to the researcher to qualitatively contrast one mode with many others. Nevertheless, the model seems to produce reasonable solution candidates and adequate data fits without much manual intervention.

5.4 Publication V: fMRI-guided multidipole localization

5.4.1 Introduction

The human visual system is anatomically and functionally organized hierarchically, so that higher-level processes modulate activity in lower levels. Therefore, it is crucial that the methods used in evaluating the sensory and cognitive processing of information are capable of resolving several close and temporally overlapping source configurations. One possibility would be to use automated dipole fitting methods, such as the one presented in Publication IV.

As our sampling method was limited by somewhat poor mixing of the samples between different modes of the multimodal posterior distribution, the use of information from other imaging methods might improve the performance. In Publication V, we introduce a novel way to incorporate fMRI information to the modeling by constructing proposal distributions for the RJMCMC sampling scheme.

Specifically, the fMRI guidance is executed by first projecting the statistical parametric maps of the fMRI results (see, Fig. 4.1 on page 25) on the source space (*i.e.*, white-gray matter boundary), then assigning some constant non-zero value to those locations that do not contain any fMRI activation, and finally normalizing the distribution to sum up to unity. This can be used as a dipole location proposal distribution affecting the acceptance ratio of the Metropolis–Hastings part of the sampling scheme so that the asymmetrically proposed jumps to locations containing fMRI activation are taken into account in the computations. If the proposed location is close to such supported by the likelihood of the MEG data, chances are that the jumps are more often accepted in the vicinity of fMRI activation leading to improved convergence. Similarly, with the reversible jumps between different number of dipoles, the fMRI-guide affects the acceptance probability of a new state *via* the proposal distribution for the new location parameters.

For a more efficient implementation, we deserted the practice of sampling the dipole location parameters as spherical angle coordinates with Metropolis–Hasting and RJMCMC. Slice sampling was still performed equivalently in spherical angle coordinates. More importantly, any kind of proposal distributions can be used without biasing the MCMC results asymptotically.

In order to reveal differences with or without the guided sampling procedure and with small errors in the proposal distribution, we constructed sets of MEG and fMRI data simulations, corresponding false positive and missing cases of fMRI detection. The simulated data were also used to examine how much faster convergence is achieved with the fMRI-guide.

We used the same drifting grating stimulus in both MEG and fMRI experiments of three participants. The drifting grating elicits visual responses first at V1 and then extending to movement area V5/MT. For qualitative evaluation of the accuracy of the obtained fMRI-guided MEG inverse solution candidates, we used multifocal mapping with fMRI to find out the individual retinotopic areas.

5.4.2 Results

With simulated data, the number of iterations required for convergence was reduced (order of 3–5) in comparison to the method without fMRI-guidance (Fig. 5.4). The clustered locations of solution candidates are more disperse with no fMRI guidance. In some cases, even though the correct fMRI information was missing, the slightly incorrect fMRI-guide still performed better than no guide at all. Our results suggest, that small errors or noisy fMRI activations will not jeopardize the localization as long as the SNR of MEG recording is good enough.

Despite the empirical clustered solutions being rather diffuse, the individual candidate solution locations coincide with the primary visual areas mapped with multifocal fMRI and to some extent also the areas close to V5/MT. In addition, the representative solution candidates produce favorable fits between the measurements and forward calculated fields (Fig. 5.5).

5.5 General discussion

5.5.1 Distributed approaches

In Publication I, the possibility of finding one specific optimal value for the ℓ^p-norm order p was examined. It was the first time such a model was implemented although ideas considering different values of p with minimum-norm estimation have been suggested (*e.g.*, Matsuura and Okabe, 1995; Beucker and Schlitt, 1996; Uutela et al., 1999; Bücker et al., 2001). Our results show that the optimal value inferred from the data varies according to such features as the source space grid discretization size, SNR of the data, and the underlying source configuration. Thus, the use of some predefined value seems arbitrary. One of the best characteristics of Bayesian formulation and evaluation in this type of model is that the samples representing the parameter posterior distribution can be used to obtain point estimates or confidence limits for the parameters of interest. An unfortunate downside is, that with distributed source estimates the source space has to contain

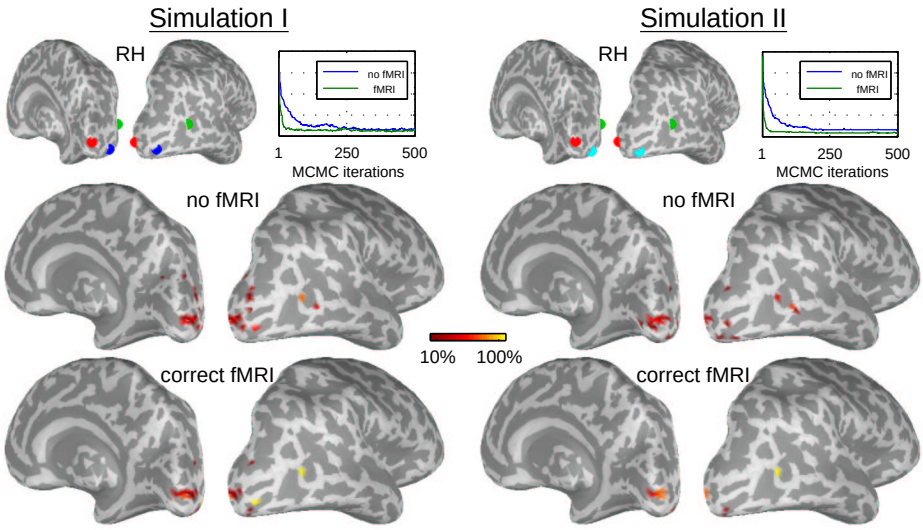

Figure 5.4: In simulations, the convergence (depicted with mean posterior energies of many chains) is faster and the clusters of solutions are less diffuse with the fMRI-guide. Color scale reveals what percentage of the chains had a dipole in that specific location.

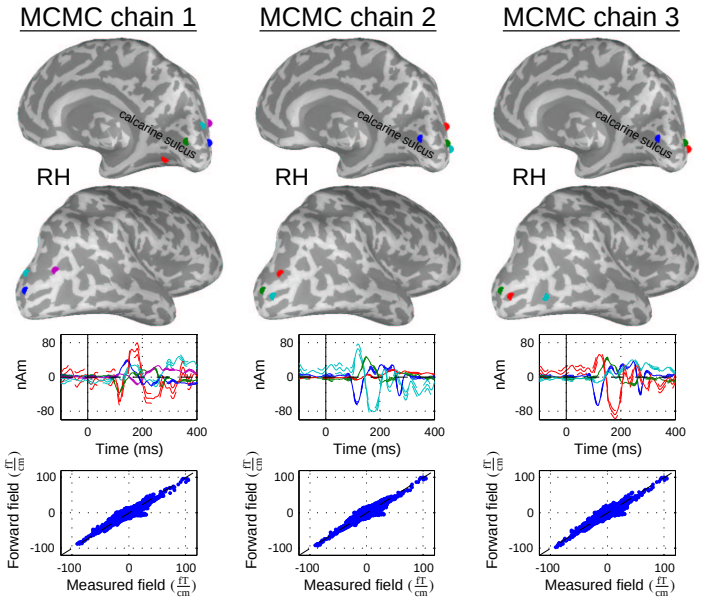

Figure 5.5: Representative solution modes and data fits of the empirical drifting grating stimulus MEG data using fMRI-guided sampling procedure.

at least approximately 3000 discretized points in order to adequately reveal anything other than just major cortical structures. Typically, big grid discretizations mean more extensive computational demands especially with numerical methods.

In many cases, the value of p was close to 1, suggesting that more focal sources would optimally explain the measured data. It seems probable that if the value of p was let to vary below 1, the sampling would still bang the lower limit and favor as small positive value as possible. This would lead to distributions with higher kurtosis (*i.e.*, peakedness) favoring solutions in which almost all the source space points contain no current and very few points yield values from the tails of the distribution. Unfortunately, this obscure effect of p banging the lower limit of 1 may well be just a manifestation of the properties of the specific model without any physiological meaning. Also, the optimal ℓ^p-norm order p for the data set presented in Publication I (close to 1), might not be optimal for a totally different data set consisting of ten or more widespread activations around the cortex. In such situations, the model might favor values of p close to 2 and yield estimates similar to the MNE.

In recent hierarchical generalization of the MNE (Sato et al., 2004), each source space point is considered to have its own precision parameter. This model was scrutinized with MCMC and VB approaches in Publications II and III. It was verified that the hierarchical MNE model results in an effective student t-distribution for the source currents, favoring focal inverse estimates in comparison to the traditional MNE. Even though the method produced rather robust estimates also with empirical data, another major issue calls for attention. The true posterior distribution as revealed by MCMC seems to be multimodal, that is, there are several possible solution candidates. The traditional MNE is unimodal while the solution depends of the selected regularization and variance parameters.

Despite that all the technical details in these models are not easily comprehended, it is important to the ordinary user to establish an understanding how specific assumptions and utilized methods affect the inverse estimates and how the results should be interpreted. For example, as one of the aims was to investigate the full distribution of solutions, the user of these methods must be careful not to draw too strict conclusions based on one single point estimate. This is of special importance as the posterior distribution in Publication II is multimodal and there are no practical ways so far to present or visualize other than one or two solution modes at a time. Note, that high multimodality was clearly observed also in Publications IV and V with the dipolar models.

One surprise with the distributed source current models was the effect that the grid discretization has on the solution. Naturally, if the number of possible source locations is decreased to a few hundred points, the accuracy of the estimates is worse than with few thousands of source space points. Even though one might consider increasing the grid discretization size as a trivial way to improve localization accuracy, at least two issues need to be considered. First, the com-

putational load for such a model in which several thousands of parameters are sampled is unbearable even with fast computers. Secondly, the model assumption of independent currents would no longer be valid if the neighboring source space points are very close to each other. Different cortical areas could be correlated with each other by introducing fMRI data to the model, for instance, or by spatial priors based on the available neuroscientific knowledge.

5.5.2 Dipole localization

The dipole localization methods in Publications IV and V are computationally feasible because the underlying sources are modeled with small number of current dipoles. This reduces the dimensionality of the parameter space considerably from the distributed current approach. The grid discretization size can be increased without affecting much of the computational aspects or the inherent properties of the model, which was not the case with the ℓ^p-norm model. The original model by Jun et al. (2005) and the ones presented in this thesis are rather automatic in comparison to traditional trial-and-error type of manual ECD fitting. In addition, the practically impossible task of globally optimizing a large number, say 5–6, dipoles to a complex data set is alleviated as the number of underlying dipoles is, in principle, possible to infer from the data by using RJMCMC sampling.

Perhaps the most profound complication emerging with the dipole localization model was already seen with the hierarchical MNE. The parameter posterior distribution proved to be highly multimodal. With computationally heavy methods, such as MCMC sampling, multimodality causes major problems as the sampling needs to be carried out for a long time before all the modes are visited. In case the sampling is not optimal some modes might not be visited at all. This leads to obvious difficulties in making statistical inferences on the parameters. If the distributions cannot be extensively charted, the conclusions may become unreliable as some solution modes of the many might not be observed at all. Importantly, the possibility of false deductions increases if the user is oblivious of the different aspects involving the interpretation of results.

As the idea with multimodal distributions is to be able to compare the probability masses of different modes, one might easily tend to believe that introducing more efficient sampling methods would ease the situation. However, methods for avoiding local convergence, such as simulated annealing or parallel tempering, may only cause unnecessary complexity to otherwise straightforward sampling. In our experience, they possibly only marginally improve the results. A more sensible remedy would be to make the model itself better by measures that may help to smooth the multimodal posterior distribution.

To the fact that our dipole sampling is still hampered by the multimodality of the posterior distribution, loosening the rigid orientation constraint (*e.g.*, Lin et al., 2006a) could prove to be useful. Based on preliminary examinations with loose

orientation constraints, in which the orientations of dipoles are allowed to slightly vary of the perpendicular with respect to the cortical mantle, the localization error caused by slight inaccuracies in the alignment of MRI and MEG coordinate frames seems to diminish (Auranen et al., 2006). Furthermore, as the posterior distribution is highly multimodal and contains spiky local modes, the loose orientation would implicitly smooth down the posterior distribution between adjacent points and that way improve the mixing properties of the sampling as it is.

With these models the researcher is, for the time being, forced to look at clustered solutions of different modes and some representative modes and make deductions of the underlying neural activity based on these. On the grounds of our empirical results and simulations presented in the publications this is, however, a practicable way of studying the brain activations. On the other hand, by performing dipole analysis the user must remember that several assumptions, such as using few point-like sources to represent all brain activations, are made already in choosing the model. This may be feasible in such a situation when there is strong prior knowledge that few focal sources should emerge from a certain type of stimulus presentation. With a more complex and "unknown" research question in mind, distributed source estimates might give at least a better starting point for interpreting the results.

With the dipole localization models the source space discretization size could be increased without adding to the computational cost. This would give a better specificity on details of the cortical white-gray matter boundary, and thus also improve localization accuracy of the dipolar sources. The proposed speed-up and regularization resort based on the SVD decomposition of the gain matrix, however, becomes heavy to compute if the dimension of the source space increases.

The speed-up strategy is needed for making the sampling scheme feasible for studies of several subjects and long data blocks. It is credible to use the SVD speed-up strategy given that nearby sensors measure at least partially the same phenomenon and some redundancy is present with the data. Nonetheless, the question of how much information is lost in this process remains partially open and more thoughtful surveys on this issue are required.

In Publication IV, the use of fMRI data for creating a proposal distribution for the reversible jump and Metropolis–Hastings parts of our MCMC sampling method was suggested. This seems to be one alternative to improve the limited mixing properties leading also to faster convergence, albeit the best results were achieved with simulated data. Despite this, it seems that slightly false fMRI activation does not mislead the sampling as long as the data is clearly visible in the MEG sensors. Conversely, our MEG simulations suggest that in case of low SNR, the correct fMRI-guidance is of help. One desirable feature of using proposal distributions with RJMCMC is the fact that it does not invalidate the theoretical considerations of MCMC. Thus, any type of proposal distribution may be used.

As a fresh idea, one might use researcher defined proposal distributions in

which the existing neuroscientific knowledge is used to weight the proposal distribution. Another way might be to create a beamformer (*e.g.*, Hillebrand and Barnes, 2003) style simple MEG data driven proposals, in which one dipole is "scanned" through the source space to form a proposal distribution based on the measurements. This is justifiable as in MEG particularly the underlying activations are located typically right beneath the sensors in which activity can be seen (not necessarily in EEG). Data driven proposal distributions might be useful in the absence of fMRI data in particular.

Based on the results presented in these publications, it seems that the most difficulties are encountered in analyzing complex experimental data. The background brain activity (*i.e.*, brain noise) might still influence the measured fields even with a large number of averages. With such a delicate forward model, in which considerable changes in the source currents may be propagated to either small or large changes in the measured fields, the background activity might cause some unexpected traits to the source estimation task. If a suitable prior for the background brain activity was constructed, a more robust examination of the underlying cortical processes might be possible. This could enable higher-level comparison of the fundamental level processes without the nuisance of unexplained background brain activity.

5.6 Future work

After the unwanted effects caused by the multimodality of the posterior distribution are suppressed, other challenges in future modeling considerations become apparent. One issue is how to calculate and visualize confidence limits and other standardized measures from the sampled representation of the posterior distribution. This will allow better conclusions based on various statistical aspects of the parameters and solutions given by the models. This is also extremely important for the practical user of the source estimation methods. Another issue is the incorporation of fMRI information also in a more profound manner than just a proposal distribution for the sampling scheme.

Recently, there have been advances in performing EEG measurements interleaved with fMRI scans (*e.g.*, Bonmassar et al., 2001), while measuring EEG simultaneously with MEG has been a routine task for some time already. With clever experimental designs, similar conditions could be made in MEG/EEG and fMRI/EEG, with EEG used for validating the interchangeability of the two experimental environments. As no fundamentally correct way of combining fMRI and MEG exists, this might serve as a way to truly integrate MEG and fMRI measurements. It is noteworthy that also EEG data by itself with the presented MEG inverse models might prove to be helpful.

Such automatic dipole fitting methods as the ones considered in this thesis

localize static dipoles, so that the actual sources are not assumed to move on the cortex. However, there is increasing interest also to dynamic models in which the sources themselves can move. Some recent ideas, for example, are based on the interpretation that dynamic nature of MEG sources prevents averaging normally used in the preprocessing phase. In these, Bayesian filtering (*i.e.*, particle filters) is employed, particularly suitable for spontaneous MEG data (*e.g.*, Somersalo et al., 2003). One of the future goals is to pursue true dynamics in the models as this might also help to understand the behavior and separation of the brain noise from the activations associated with sensory stimulation and intrinsic cognitive processes.

Chapter 6

Summary

In this study, novel ideas and improvements to the inverse estimation of neuromagnetic sources were presented using computational methods and Bayesian data analysis. Both anatomical and functional MRI data were used in the modeling. The empirical experiments and simulations performed for testing the models were tightly connected to real neuroscience data. All the proposed methods are relatively automatic and require little or no manual intervention, although a good understanding of the properties of the models involved is needed in order to avoid false interpretations by the ordinary user. Whereas the sampling of the distributed source current parameters may be computationally overly intensive, the sampling of location and number of dipolar sources seems as a good alternative to this. The performance of the dipole localization with MCMC, however, is deteriorated by the presence of an apparently highly multimodal parameter posterior distribution. Even with additional prior information from fMRI measurements in guiding the algorithm, the dipole sampling seems to have somewhat limited mixing properties. In our experience, it appears unlikely that trying to improve the sampling method as it is will be successful. Loosening the strict orientation constraint instead or utilizing other ways for smoothing the spikedness and multimodality of the posterior distribution might be much more fruitful in future endeavors. It will also be extremely important to develop the visualization of the distribution of solutions for making the interpretation of results easier for the user.

References

Ahlfors, S. P. and Simpson, G. V. (2004). Geometrical interpretation of fMRI-guided MEG/EEG inverse estimates. *NeuroImage*, 22:323–332.

Ahlfors, S. P., Simpson, G. V., Dale, A. M., Belliveau, J. W., Liu, A. K., Korvenoja, A., Virtanen, J., Huotilainen, M., Tootell, R. B. H., Aronen, H. J., and Ilmoniemi, R. J. (1999). Spatiotemporal activity of a cortical network for processing visual motion revealed by MEG and fMRI. *Journal of Neurophysiology*, 82(5):2545–2555.

Auranen, T., Nummenmaa, A., Hämäläinen, M. S., Jääskeläinen, I. P., Lampinen, J., Vehtari, A., and Sams, M. (2006). Cortically constrained neuromagnetic inverse analysis: Structure of Bayesian multidipolar solutions and effects of MEG-fMRI coregistration error. In 12th Annual Meeting of the Organization for Human Brain Mapping, June 11–15, Florence, Italy.

Baillet, S. and Garnero, L. (1997). A Bayesian approach to introducing anatomo-functional priors in the EEG/MEG inverse problem. *IEEE Transactions on Biomedical Engineering*, 44(5):374–385.

Baillet, S., Garnero, L., Marin, G., and Hugonin, J.-P. (1999). Combined MEG and EEG source imaging by minimization of mutual information. *IEEE Transactions on Biomedical Engineering*, 46(5):522–534.

Baillet, S., Mosher, J. C., and Leahy, R. M. (2001). Electromagnetic brain mapping. *IEEE Signal Processing Magazine*, 18(6):14–30.

Bandettini, P. A., Wong, E. C., Hinks, R. S., Tikofsky, R. S., and Hyde, J. S. (1992). Time course EPI of human brain function during task activation. *Magnetic Resonance in Medicine*, 25:390–397.

Belliveau, J. W., Kennedy, D. N. J., McKinstry, R. C., Buchbinder, B. R., Weisskoff, R. M., Cohen, M. S., Vevea, J. M., Brady, T. J., and Rosen, B. R. (1991). Functional mapping of the human visual cortex by magnetic resonance imaging. *Science*, 254:716–719.

Bernardo, J. M. and Smith, A. F. M. (2000). *Bayesian Theory*. John Wiley & Sons, Ltd.

Bertrand, C., Hamada, Y., and Kado, H. (2001a). MRI prior computation and parallel tempering algorithm: A probabilistic resolution of the MEG/EEG inverse problem. *Brain Topography*, 14(1):57–68.

Bertrand, C., Ohmi, M., Suzuki, R., and Kado, H. (2001b). A probabilistic solution to the MEG inverse problem via MCMC methods: The reversible jump and parallel tempering algorithms. *IEEE Transactions on Biomedical Engineering*, 48(5):533–542.

Beucker, R. and Schlitt, H. A. (1996). On minimal ℓ_p-norm solutions of the biomagnetic inverse problem. Technical Report KFA-ZAM-IB-9614, Research Center Jülich, Germany.

Bonmassar, G., Schwartz, D. P., Liu, A. K., Kwong, K. K., Dale, A. M., and Belliveau, J. W. (2001). Spatiotemporal brain imaging of visual-evoked activity using interleaved EEG and fMRI recordings. *NeuroImage*, 13:1035–1043.

Box, G. E. P. and Tiao, G. C. (1973). *Bayesian Inference in Statistical Analysis*. John Wiley and Sons, Inc.

Brenner, D., Lipton, J., Kaufman, L., and Williamson, S. J. (1978). Somatically evoked magnetic fields of the human brain. *Science*, 199:81–83.

Brenner, D., Williamson, S. J., and Kaufman, L. (1975). Visually evoked magnetic fields of the human brain. *Science*, 190:480–482.

Brooks, S. P. and Gelman, A. (1998). General methods for monitoring convergence of iterative simulations. *Journal of Computational and Graphical Statistics*, 7(4):434–455.

Brooks, S. P., Giudici, P., and Roberts, G. O. (2003). Efficient construction of reversible jump Markov chain Monte Carlo proposal distributions. *Journal of Royal Statistical Society B*, 65:1–37.

Bücker, H. M., Beucker, R., and Bischof, C. H. (2001). Using automatic differentiation for the minimal p-norm solution ot the biomagnetic inverse problem.

Clarke, C. J. S. (1989). Probabilistic methods in a biomagnetic inverse problem. *Inverse Problems*, 5:999–1012.

Cohen, D. (1968). Magnetoencephalography: Evidence of magnetic fields produced by alpha-rhythm currents. *Science*, 161:784–786.

Cohen, D. (1972). Magnetoencephalograhpy: Detection of the brain's electrical activity with a superconducting magnetometer. *Science*, 175:664–666.

Cohen, D., Edelsack, E. A., and Zimmerman, J. E. (1970). Magnetocardiograms taken inside a shielded room with a superconducting point-contact magnetometer. *Applied Physics Letters*, 16(7):278–280.

Courtney, S. M. and Ungerleider, L. G. (1997). What fMRI has taught us about human vision. *Current Opinion in Neurobiology*, 7:554–561.

Dale, A. M. (1999). Optimal experimental design for event-related fMRI. *Human Brain Mapping*, 8:109–114.

Dale, A. M., Fischl, B., and Sereno, M. I. (1999). Cortical surface-based analysis I: Segmentation and surface reconstruction. *NeuroImage*, 9:179–194.

Dale, A. M., Liu, A. K., Fischl, B. R., Buckner, R. L., Belliveau, J. W., Lewine, J. D., and Halgren, E. (2000). Dynamic statistical parametric mapping: Combining fMRI and MEG for high-resolution imaging of cortical activity. *Neuron*, 26:55–67.

Dale, A. M. and Sereno, M. I. (1993). Improved localization of cortical activity by combining EEG and MEG with MRI cortical surface reconstruction: A linear approach. *Journal of Cognitive Neuroscience*, 5(2):162–176.

DeYoe, E. A., Carman, G. J., Bandettini, P., Glickman, S., Wieser, J., Cox, R., Miller, D., and Neitz, J. (1996). Mapping striate and extrastriate visusal areas in human cerebral cortex. *Proceedings of the National Academy of Sciences of the United States of America*, 93:2382–2386.

Dougherty, R. F., Koch, V. M., Brewer, A. A., Fischer, B., Modersitzki, J., and Wandell, B. A. (2003). Visual field representations and locations of visual areas V1/2/3 in human visual cortex. *Journal of Vision*, 3:586–598.

Engel, S. A., Glover, G. H., and Wandell, B. A. (1997). Retinotopic organization in human visual cortex and the spatial precision of functional MRI. *Cerebral Cortex*, 7:181–192.

Farrell, D. E., Tripp, J. H., Nogren, R., and Teyler, T. J. (1980). A study of the auditory evoked magnetic field of the human brain. *Electroencephalography and Clinical Neurophysiology*, 49:31–37.

Fischl, B., Liu, A., and Dale, A. M. (2001). Automated manifold surgery: Constructing geometrically accurate and topologically correct models of the human cerebral cortex. *IEEE Transactions on Medical Imaging*, 20(1):70–80.

Fischl, B., Sereno, M. I., and Dale, A. M. (1999). Cortical surface-based analysis II: Inflation, flattening, and a surface-based coordinate system. *NeuroImage*, 9:195–207.

Gelfand, A. E. and Ghosh, S. K. (1998). Model choice: A minimum posterior predictive loss approach. *Biometrika*, 85(1):1–11.

Gelman, A., Carlin, J. B., Stern, H. S., and Rubin, D. B. (2003). *Bayesian Data Analysis*. Chapman & Hall/CRC, second edition.

Geman, S. and Geman, D. (1984). Stochastic relaxation, Gibbs distributions, and the Bayesian restoration of images. *IEEE Transactions on Pattern Analysis and Machine Intelligence*, 6(6):721–741.

Ghahramani, Z. and Beal, M. (2001). *Graphical Models and Variational Methods*. In *Advanced Mean Field Methods — Theory and Practice*, M. Opper and D. Saad. (editors), MIT Press.

Gilks, W. R., Richardson, S., and Spiegelhalter, D. J. (1996). *Markov chain Monte Carlo in Practice*. Chapman & Hall.

Green, P. J. (1995). Reversible jump Markov chain Monte Carlo computation and Bayesian model determination. *Biometrika*, 82(4):711–732.

Hari, R., Aittoniemi, K., Järvinen, M.-L., Katila, T., and Varpula, T. (1980). Auditory evoked transient and sustained magnetic fields of the human brain: Localization of neural generators. *Experimental Brain Research*, 40:237–240.

Hastings, W. K. (1970). Monte Carlo sampling methods using Markov chains and their applications. *Biometrika*, 57(1):97–109.

Hauk, O. (2004). Keep it simple: A case for using classical minimum norm estimation in the analysis of EEG and MEG data. *NeuroImage*, 21:1612–1621.

Hillebrand, A. and Barnes, G. R. (2003). The use of anatomical constraints with MEG beamformers. *NeuroImage*, 20:2302–2313.

Huettel, S. A., Song, A. W., and McCarthy, G. (2004). *Functional Magnetic Resonance Imaging*. Sinauer.

Hämäläinen, M. S., Hari, R., Ilmoniemi, R. J., Knuutila, J., and Lounasmaa, O. V. (1993). Magnetoencephalography — theory, instrumentation, and applications to noninvasive studies of the working human brain. *Reviews of Modern Physics*, 65(2):413–497.

Hämäläinen, M. S. and Ilmoniemi, R. J. (1984). Interpreting measured magnetic fields of the brain: Estimates of current distributions. Technical Report TKK-F-A559, Helsinki University of Technology, Department of Technical Physics.

Hämäläinen, M. S. and Ilmoniemi, R. J. (1994). Interpreting magnetic fields of the brain: Minimum norm estimates. *Medical and Biological Engineering and Computing*, 32(1):35–42.

Hämäläinen, M. S. and Sarvas, J. (1989). Realistic conductivity geometry model of the human head for interpretation of neuromagnetic data. *IEEE Transactions on Biomedical Engineering*, 36(2):165–171.

Ilmoniemi, R. J. (1994). Magnetic source imaging. *Biological Effects of Electric and Magnetic Fields*, 2:49–79.

Ioannides, A. A., Bolton, J. P. R., and Clarke, C. J. S. (1990). Continuous probabilistic solutions to the biomagnetic inverse problem. *Inverse Problems*, 6:523–542.

Jun, S. C., George, J. S., Paré-Blagoev, J., Plis, S. M., Ranken, D. M., Schmidt, D. M., and Wood, C. C. (2005). Spatiotemporal Bayesian inference dipole analysis for MEG neuroimaging data. *NeuroImage*, 28:84–98.

Jun, S. C., George, J. S., Plis, S. M., Ranken, D. M., Schmidt, D. M., and Wood, C. C. (2006). Improving source detection and separation in a spatiotemporal Bayesian inference dipole analysis. *Physics in Medicine and Biology*, 51:2395–2414.

Kandel, E. R., Schwartz, J. H., and Jessell, T. M. (2000). *Principles of Neural Science*. McGraw-Hill, fourth edition.

Kincses, W. E., Braun, C., Kaiser, S., Grodd, W., Ackermann, H., and Mathiak, K. (2003). Reconstruction of extended cortical sources for EEG and MEG based on a Monte-Carlo-Markov-chain estimator. *Human Brain Mapping*, 18:100–110.

Kwong, K. K., Belliveau, J. W., Chesler, D. A., Goldberg, I. E., Weisskoff, R. M., Poncelet, B. P., Kennedy, D. N., Hoppel, B. E., Cohen, M. S., Turner, R., Cheng, H.-M., Brady, T. J., and Rosen, B. R. (1992). Dynamic magnetic resonance imaging of human brain activity during primary sensory stimulation. *Proceedings of the National Academy of Sciences of the United States of America*, 89:5675–5679.

Köhler, T., Wagner, M., Fuchs, M., Wischmann, H.-A., Drenckhahn, R., and Theissen, A. (1996). Depth normalization in MEG/EEG current density imaging. In *Proceedings of the 18th Annual International Conference of the IEEE Engineering in Medicine and Biology Society*.

Lin, F.-H., Belliveau, J. W., Dale, A. M., and Hämäläinen, M. S. (2006a). Distributed current estimates using cortical orientation constraints. *Human Brain Mapping*, 27(1):1–13.

Lin, F.-H., Witzel, T., Ahlfors, S. P., Stufflebeam, S. M., Belliveau, J. W., and Hämäläinen, M. S. (2006b). Assessing and improving the spatial accuracy in MEG source localization by depth-weighted minimum-norm estimates. *NeuroImage*, 31:160–171.

Liu, A. K., Belliveau, J. W., and Dale, A. M. (1998). Spatiotemporal imaging of human brain activity using functional MRI constrained magnetoencephalography data: Monte Carlo simulations. *Proceedings of the National Academy of Sciences of the United States of America*, 95:8945–8950.

Liu, A. K., Dale, A. M., and Belliveau, J. W. (2002). Monte Carlo simulation studies of EEG and MEG localization accuracy. *Human Brain Mapping*, 16:47–62.

Logothetis, N. K., Pauls, J., Augath, M., Trinath, T., and Oeltermann, A. (2001). Neurophysiological investigation of the basis of the fMRI signal. *Nature*, 412:150–157.

Lütkenhöner, B. (1992). Frequency-domain localization of intracerebral dipolar sources. *Electroencephalography and Clinical Neurophysiology*, 82:112–118.

Matsuura, K. and Okabe, Y. (1995). Selective minimum-norm solution of the biomagnetic inverse problem. *IEEE Transactions on Biomedical Engineering*, 42(6):608–615.

Matsuura, K. and Okabe, Y. (1997). A robust reconstruction of sparse biomagnetic sources. *IEEE Transactions on Biomedical Engineering*, 44(8):720–726.

Metropolis, N., Rosenbluth, A. W., Rosenbluth, M. N., Teller, A. H., and Teller, E. (1953). Equation of state calculations by fast computing machines. *The Journal of Chemical Physics*, 21(6):1087–1092.

Mosher, J. C., Leahy, R. M., and Lewis, P. S. (1999). EEG and MEG: Forward solutions for inverse methods. *IEEE Transactions on Biomedical Engineering*, 46(3):245–259.

Mosher, J. C., Lewis, P. S., and Leahy, R. M. (1992). Multiple dipole modeling and localization from spatio-temporal MEG data. *IEEE Transactions on Biomedical Engineering*, 39(6):541–557.

Neal, R. M. (1996). *Bayesian Learning for Neural Networks*. Springer-Verlag.

Neal, R. M. (2003). Slice sampling. *The Annals of Statistics*, 31(3):705–767.

Niedermeyer, E. and Silva, F. L. D. (1999). *Electroencephalography: Basic Principles, Clinical Applications, and Related Fields*. Lippincott Williams & Wilkins, fourth edition.

Ogawa, S., Tank, D. W., Menon, R., Ellermann, J. M., Kim, S., Merkle, H., and Ugurbil, K. (1992). Intrinsic signal changes accompanying sensory stimulation: Functional brain mapping with magnetic resonance imaging. *Proceedings of the National Academy of Sciences of the United States of America*, 89:5951–5955.

Okada, Y. C., Wu, J., and Kyuhou, S. (1997). Genesis of MEG signals in a mammalian CNS structure. *Electroencephalography and Clinical Neurophysiology*, 103:474–485.

Ollikainen, J. O., Vauhkonen, M., Karjalainen, P. A., and Kaipio, J. P. (1999). Effects of local skull inhomogeneities on EEG source estimation. *Medical Engineering & Physics*, 21:143–154.

Pascual-Marqui, R. D. (2002). Standardized low resolution brain electromagnetic tomography (sLORETA): Technical details. *Methods & Findings in Experimental & Clinical Pharmacology*, 24:5–12.

Phillips, C., Mattout, J., Rugg, M. D., Maquet, P., and Friston, K. J. (2005). An empirical Bayesian solution to the source reconstruction problem in EEG. *NeuroImage*, 24:997–1011.

Phillips, C., Rugg, M. D., and Friston, K. J. (2002a). Anatomically informed basis functions for EEG source localization: Combining functional and anatomical constraints. *NeuroImage*, 16:678–695.

Phillips, C., Rugg, M. D., and Friston, K. J. (2002b). Systematic regularization of linear inverse solutions of the EEG source localization problem. *NeuroImage*, 17:287–301.

Phillips, J. W., Leahy, R. M., and Mosher, J. C. (1997). MEG-based imaging of focal neuronal current sources. *IEEE Transactions on Medical Imaging*, 16(3).

Reite, M., Edrich, J., Zimmerman, J. T., and Zimmerman, J. E. (1978). Human magnetic auditory evoked fields. *Electroencephalography and Clinical Neurophysiology*, 45:114–117.

Robert, C. P. and Casella, G. (2004). *Monte Carlo Statistical Methods*. Springer, second edition.

Romani, G. L., Williamson, S. J., and Kaufman, L. (1982). Tonotopic organization of the human auditory cortex. *Science*, 216:1339–1340.

Salmelin, R. H. and Hämäläinen, M. S. (1995). Dipole modelling of MEG rhythms in time and frequency domains. *Brain Topography*, 7(3):251–257.

Sarvas, J. (1987). Basic mathematical and electromagnetic concepts of the biomagnetic inverse problem. *Physics in Medicine and Biology*, 32(1):11–22.

Sato, M.-A., Yoshioka, T., Kajihara, S., Toyama, K., Goda, N., Doya, K., and Kawato, M. (2004). Hierarchical Bayesian estimation for MEG inverse problem. *NeuroImage*, 23:806–826.

Schmidt, D. M., George, J. S., Ranken, D. M., and Wood, C. C. (2000). Spatial-temporal Bayesian inference for MEG/EEG. In *Biomag 2000: 12th International Conference on Biomagnetism, Espoo, Finland*.

Schmidt, D. M., George, J. S., and Wood, C. C. (1999). Bayesian inference applied to the electromagnetic inverse problem. *Human Brain Mapping*, 7:195–212.

Sereno, M. I., Dale, A. M., Reppas, J. B., Kwong, K. K., Belliveau, J. W., Brady, T. J., Rosen, B. R., and Tootell, R. B. H. (1995). Borders of multiple visual areas in humans revealed by functional magnetic resonance imaging. *Science*, 268:889–893.

Smith, S. M., Jenkinson, M., Woolrich, M. W., Beckmann, C. F., Behrens, T. E. J., Johansen-Berg, H., Bannister, P. R., Luca, M. D., Drobnjak, I., Flitney, D. E., Niazy, R. K., Saunders, J., Vickers, J., Zhang, Y., Stefano, N. D., Brady, J. M., and Matthews, P. M. (2004). Advances in functional and structural MR image analysis and implementation as FSL. *NeuroImage*, 23:S208–S219.

Somersalo, E., Voutilainen, A., and Kaipio, J. P. (2003). Non-stationary magnetoencephalography by Bayesian filtering of dipole models. *Inverse Problems*, 19:1047–1063.

Teyler, T. J., Cuffin, B. N., and Cohen, D. (1975). The visual evoked magnetoencephalogram. *Life Sciences*, 17:683–692.

Uutela, K., Hämäläinen, M. S., and Somersalo, E. (1999). Visualization of magnetoencephalographic data using minimum current estimates. *NeuroImage*, 10:173–180.

Vrba, J. and Robinson, S. E. (2001). Signal processing in magnetoencephalography. *Methods*, 25:249–271.

Wang, J.-Z., Williamson, S. J., and Kaufman, L. (1992). Magnetic source images determined by a lead-field analysis: The unique minimum-norm least-squares estimation. *IEEE Transactions on Biomedical Engineering*, 39(7):665–675.

Zimmerman, J. E. (1977). SQUID instruments and shielding for low-level magnetic measurements. *Journal of Applied Physics*, 48(2):702–710.

ISBN 978-951-22-8953-0 (printed)
ISBN 978-951-22-8954-7 (PDF)
ISSN 1455-0474

PicaSet Oy, Helsinki 2007